ChemPubSoc Europe

DOI: 10.1002/ejic.201900756

EurJIC European Journal of Inorganic Chemistry

Minireview

Perovskite Nitrides | *Very Important Paper* |

VIP Metal-Rich Ternary Perovskite Nitrides

and Rainer Niewa*[a]

Abstract: Research interest in inverse perovskite nitrides, since the early beginnings in the 1940s has considerably intensified in recent years. Within the last decades exploration lead to a wide variety of new compounds, compositions and structural arrangements. Electronic properties of the novel materials span from insulating and semiconducting via semimetallic and metallic, depending on element combination. Similarly, magnetic properties qualify for various applications, according to frequently high Curie temperatures and saturation magnetizations, together with development of delicate magnetic structures and often occurring metamagnetic transitions, to give only few examples. This minireview is intended to give an overview on formation of such metal-rich compounds with focus on chemical systems and crystal chemistry.

1. Introduction

Since the early discovery of the mineral perovskite by *Gustav Rose* in 1839,[1] named after the Russian politician, war veteran, mineral collector and supporter of sciences like mineralogy and archeology, *Count Lev Aleksevich von Perovski*, and the detailed structural characterization of "$CaTiO_3$ and related compounds" inspired by *Victor Moritz Goldschmidt*, conducted in Oslo by his students *Thomas F. W. Barth* and *Frederik W. H. Zachariasen*,[2] a steadily increasing number of particularly ternary metal oxides are referred to as perovskites of different types. Common to all oxides termed perovskites is the close structural relation with the ideal ABO_3 cubic structure depicted in Figure 1, composed by all-corner-sharing $BO_{6/2}$ octahedra creating a framework, in which the larger *A* cations reside in cuboctahedral interstitial voids. The framework of $BO_{6/2}$ octahedra presents highly flexible, resulting in numerous distortion variants of lower symmetry produced by rotation and tilting of these octahedra, where the size of the *A* cations allows.[3] Additionally, the octahedra may be distorted due to different reasons like, for example, Jahn–Teller effect or displacement of the central *B* atom. Apart from distortion variants, non-cubic stacking of closed packed AO_3-layers, which can be regarded as a second fundamental structural motif of the perovskite structure, leads to so-called hexagonal perovskites with various fractions of face-sharing octahedra $BO_{6/2}$.[4] Furthermore, layered and intergrowth derivatives of deviating general composition occur when layered sections of the perovskite structure are separated by further

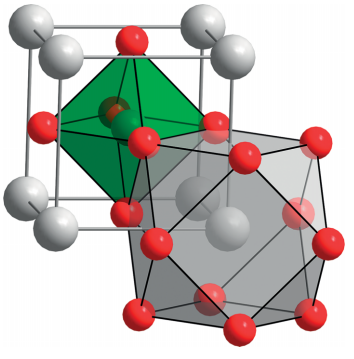

Figure 1. Crystal structure of a cubic perovskite. For inverse Peroskite nitrides, nitrogen (green sphere) is located in all vertex-sharing octahedra from rather nitrophilic metal atoms (red), while typically larger and less nitrophilic metal or metametal atoms (gray) reside in cuboctahedral coordination by twelve metal atoms of the first kind. One common unit cell choice is indicated by gray lines.

[a] *Institut für Anorganische Chemie, Universität Stuttgart, Pfaffenwaldring 55, 70569 Stuttgart, Germany*
E-mail: rainer.niewa@iac.uni-stuttgart.de
www.iac.uni-stuttgart.de
ORCID(s) from the author(s) for this article is/are available on the WWW under https://doi.org/10.1002/ejic.201900756.

Rainer Niewa studied chemistry at the Universities of Essen and Dortmund, Germany. In Dortmund he also earned his diploma and doctoral degrees with topics of inorganic solid state chemistry. After a postdoctoral stay at the Cornell University in Ithaca, New York, he moved to the newly founded Max Planck Institute for Chemical Physics of Solids in Dresden. In 2005 he finished his habilitation at the Technical University of Dresden and accepted a position as Professor for Synthesis and Characterization of Innovative Materials at the Technical University of Munich. Since 2009 he is Professor for Inorganic Chemistry at the University of Stuttgart. The focus of his research includes the synthesis of new inorganic materials employing a broad spectrum of synthesis techniques and the characterization of these materials in terms of composition, crystal structure, and relevant physical properties.

structural motifs. All these hexagonal and layered perovskite-variants can again be subject to distortion to lower symmetry via deformation, tilting and rotation of octahedra. The intrinsic flexibility and versatility of the perovskite structure allows the formation of a wide number of derivatives, polymorphs and superstructures, as well as the introduction of defects and structural disorder.

In the common oxidic perovskites the relative sizes of the *A* and *B* cations for a given temperature govern the degree of structural distortion with respect to the ideal cubic structure. The relationship between the structure and the ionic radii of these ions was rationalized by *V. M. Goldschmidt*, who derived the tolerance factor, *t*, from purely geometric considerations according to

$$t = \frac{r(A) + r(\mathrm{O})}{\sqrt{2}(r(B) + r(\mathrm{O}))}$$

where $r(A)$, $r(B)$ and $r(\mathrm{O})$ are the radii of the different ions.[5] The cubic perovskite structure forms for values *t* of close to unity. For values below 1, meaning the *A* cations are not able to effectively fill the cuboctahedral voids, the vacant space in the structure is minimized by tilting of the corner-sharing BO_6 octahedra. At room temperature a value of $t = 0.89$ is generally accepted as boundary, below which tilt structures with symmetries lower than cubic are expected. For values even less than roughly $t = 0.80$ the perovskite structure typically collapses to different arrangements like Ilmenite, Corundum or else.[6] In case of *A* cations too large for the three-dimensional framework of BO_6 octahedra, i.e. $t > 1.02$, strain is released by transforming to hexagonal perovskites, where some of the octahedra share faces.

Many such perovskite-materials exhibit interesting and intriguing properties of various kinds. Development paved the way to principally new perovskite-based technologies and thus have found numerous applications in highly diverse areas of daily life, like in solar cells or as ferro-, piezo- or dielectrics in capacitors, actuators, acoustic transformers and transducers, high-temperature superconductors, proton conductors, fuel cells, memory storage devices, or colossal magnetoresistors.[e.g. 7] This broad extend of applications is partially made possible by the high structural flexibility in combination with an extremely wide range of feasible element combinations: All three positions within the ABO_3 general composition are versatile to substitution with larger (*A*) and smaller (*B*) cations (including polyatomic complex or organic ions), respectively, and by anions (O) like fluoride, chloride or nitride, to name only few, resulting in a plethora of different properties depending on element combination and crystal structure details.

The extreme stability of the perovskite motif partially relates to the high Madelung constant of the structural arrangement.[8] Consequently, any ionic perovskite with inverted ionic charges delivers an equally high Madelung constant. Therefore, it is not surprising that the perovskite arrangement can be found similarly for a large variety of compounds $(M_3Z)E$ with *M* representing a cation located on the oxide position of the classical perovskite structure and *Z* an anion on the *B* site. *Z* frequently is exemplified by B, C, O, or N. In this review, we will concentrate solely on inverse (anti-)perovskite nitrides with *Z* = N, where three large groups of substances may be identified, depending on the type of *E* on the *A* position, the chemical nature of which relates to those of *Z* and *M*: *i*) For real anionic metalloids like group fifteen or group fourteen ions, $E(15)^{3-}$ or $E(14)^{4-}$, respectively, predominantly semiconducting compounds with dominating ionic bonding occur, if *M* is represented by alkaline-earth metal ions. *ii*) If *M* is a rare-earth metal, rather metallic nitrides form, with *E* again mostly from choice of main-group metals or metalloids. *iii*) Finally, a particularly large group of metallic compounds is composed by transition metal atoms on the *M* position and either a further transition metal or a main-group metal or metalloid on the *E* site.

In the following *M* will generally be used as a placeholder for a metal, preferentially for a transition metal, *A* will stand for alkaline-earth metals, *R* for rare-earth metals and *E* for main-group metals and metalloids. The symbol *Z* will occasionally be utilized for the nonmetallic elements B, C, N, O.

2. Inverse Perovskite Nitrides of the Alkaline-Earth Metals

Compounds in this section mostly concern the combinations of alkaline-earth metals with metametals from main groups 13–15 from the periodic systems of the elements. The solely compound with transition metals known to date is $(Ca_3N)Au$. Additionally, the alkali metal variants $Li(Ba_3N)$ and $Na(Ba_3N)$ were reported. In this section the largest variation of crystal structure details can be found, comprising cubic perovskites and distortion variants thereof, vacancy ordered elpasolites, hexagonal perovskites and Ruddlesden–Popper phases. Additionally, the electronic situation spans from insulators and semiconductors all the way to metallic compounds.

2.1. Inverse Perovskite Nitrides with Group 15 Elements: $(A_3N)E(15)$ and Related Phases

Alkaline-earth metal perovskite nitrides of the group 15 elements *E* = P, As, Sb, Bi all exhibit full nitrogen site occupation and thus a general composition $(A_3N)E$, which might be rationalized by a fully ionic picture according to $(A^{2+})_3(N^{3-})(E^{3-})$. Correspondingly, all compounds are semiconducting. The compounds of the lighter elements, P and As, in combination with lighter alkaline-earth metals are even colored yellow, orange and red [$(Mg_3N)As$, $(Ca_3N)P$, $(Ca_3N)As$], while those constituting of heavier elements are rather gray to black.[9–11] All compounds represent diamagnetic semiconductors according to both experimental property determinations and electronic structure calculations, while findings like weak paramagnetism or slight metallic temperature characteristic of the electrical resistivity might be due to impurities and vacancies in the alkaline-earth metal substructure.[11–13] Recently, DFT calculations revealed potential for thermoelectric and photovoltaic applications[14,15] as well as the presence of topological insulators and Dirac semimetals, if properly strained,[16] but experimental confirmation was not yet realized. At ambient conditions, $(Mg_3N)E$ with *E* = As, Sb, $(Ca_3N)E$ and $(Sr_3N)E$ with *E* = Sb, Bi

have been reported to crystallize in the ideal cubic perovskite structure.[9,11,12,17] Similar to the classical oxide perovskites, distortions from cubic were observed for the smaller ions, P^{3-} and As^{3-}, located within the (deformed) cuboctahedral voids, so far exclusively arriving at the orthorhombic $GdFeO_3$ structure type (space group *Pnma*).[11,18] For the series $(A_3N)As$ with *A* = Mg, Ca, Sr, Ba the distortion was recently analyzed to monotonically increase with rising ionic radius of the alkaline-earth metal ion, due to the increasing size of the cuboctahedral void upon unit cell enlargement and despite the growing spatial requirement of the A^{2+} ions (see Figure 2). A quantification of the distortion based on a simple analysis of the local coordination polyhedra revealed the deviation from ideal cubic structure to be nearly exclusively due to distortion of the cuboctahedral surrounding of As^{3-}, demonstrating the rigidity of the A_6N-octahedra.[10,19] An analogous situation in terms of composition, electrical properties and structural relationships is realized for the group 14 element oxides $(A_3O)E(14)$ [*A* = Ca, Sr, Ba, Eu, Yb; *E*(14) = Si, Ge, Sn, Pb].[20–25]

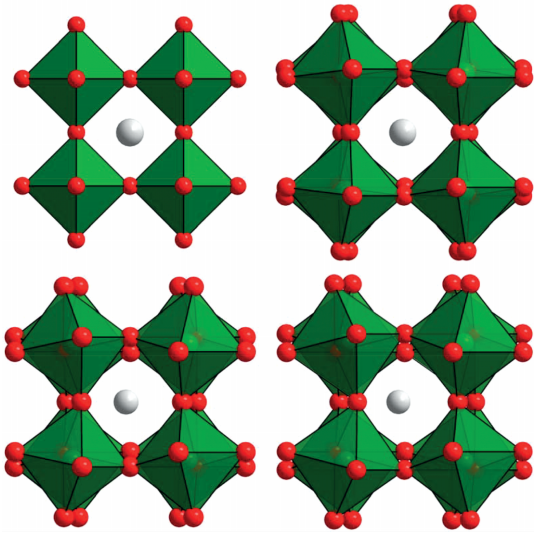

Figure 2. Crystal structures of a cubic perovskite and increasing orthorhombic distortion (space group *Pnma*) upon increasing alkaline-earth metal radius in $(A_3N)As$: $(Mg_3N)As$ top left, $(Ca_3N)As$ top right, $(Sr_3N)As$ bottom left, $(Ba_3N)As$ bottom right (N: green spheres, *E*: gray spheres, *A*: red spheres).

The compounds $(Ba_3N)E$ with the larger *E* = Sb, Bi crystallize in the hexagonal 2H-perovskite variant ($BaNiO_3$ structure type, see Figure 3), although the Goldschmidt tolerance factor should even decrease compared to the respective cubic strontium or calcium compounds.[12,26] A reason for a stabilization of the hexagonal structure variant for particularly the barium compounds may be seen in a local shielding of the Coulomb repulsion between the alike charged nitride ions within face-sharing octahedral by the larger and softer (according to HSAB concept) barium ions. Still, in the crystal structures, these octahedra Ba_6N are elongated parallel to [001]. Interesting isotypes of these hexagonal perovskite nitrides are represented by the metallic subnitrides $Li(Ba_3N)$ and $Na(Ba_3N)$, with Li and Na replacing the metalloid *E*, similarly suffering from highly elongated octahedra.[27]

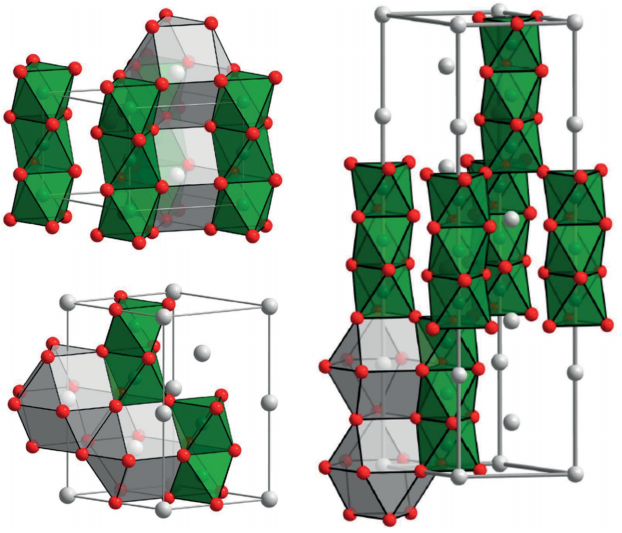

Figure 3. Crystal structures of hexagonal perovskite variants (N: green spheres, *E*: gray spheres, *A*: red spheres): 2H-perovskite observed for $(Ba_3N)E(15)$ with *E* = Sb and Bi ($BaNiO_3$-type structure, top left), $(Sr_{3-x}Ba_xN)E(15)$ with around $x = 1.5$ and 4*H*-perovskite structure ($BaMnO_3$-type structure, bottom left) and with $x \approx 2.3$ and 9R-perovskite arrangement ($BaRuO_3$-type structure, right).

Quaternary solid solutions of the type $(Sr_{3-x}Ba_xN)E(15)$ crystallize in stacking variants of such hexagonal and cubic perovskites depending on the Sr/Ba ratio (Figure 3).[28] For *E* = Bi the quaternary system reveals a homogeneity range around $x = 1.5$ (approximate range $1.3 \le x \le 2.0$, depending on temperature), in which a 4*H*-perovskite ($BaMnO_3$-type) is observed. With higher Ba content of around $x \approx 2.3$ a 9R arrangement ($BaRuO_3$-type) is realized. The vertices of octahedra $A_{6/2}N$ are preferentially occupied by Sr if vertex-sharing like in the cubic compound $(Sr_3N)Bi$, while rather consist of Ba when face-sharing as in the hexagonal perovskite $(Ba_3N)Bi$. These crystal structures can be rationalized as ordered intergrowth or stacking variants of the ideal cubic and the hexagonal 2H-perovskite with all corner-sharing octahedra ($Sr_{6/2}N$) and all face-sharing octahedra ($Ba_{6/2}N$), respectively.

Furthermore, an inverse Ruddlesden–Popper series of the general composition $(A_{3n+1}Z_n)Bi_{n+1}$ with *Z* = N, O and *n* = 1, 3 was observed.[29] Crystal structure arrangements are depicted in Figure 4. For $Z = (n - 1)$ N and 1 O the composition transforms to $(A_{3n+1}ON_{n-1})Bi_{n+1}$. Given A^{2+} and Bi^{3-} in the ionic limit, this general composition accords to charge balance. For the classical Ruddlesden–Popper series $Sr_{1+n}Ti_nO_{3n+1}$ the popular formula $n\ SrTiO_3 \cdot SrO$ underlines the intergrowth of structural sections of cubic perovskite and rocksalt type, respectively. In analogy, the inverse Ruddlesden–Popper phases correspond to $n\ (A_3ON_{n-1})Bi \cdot ABi$, with the latter bismuthide ions located in an interlayer site with capped square antiprismatic coordination being regarded a part of the rocksalt type structural part. We note the perovskite composition $(A_3N)Bi$ as the end member of this series for $n \to \infty$.

In fact, the perovskite derivatives $((Ba_{1-x}Sr_x)_4O)Bi_2$ and $((Ba_{1-x}Sr_x)_{10}N_2O)Bi_4$ were obtained as solid solutions of the purely Sr and Ba containing compounds. The *n* = 1 phase $((Ba_{1-x}Sr_x)_4O)Bi_2$ crystallizes in the K_2NiF_4 structure type with

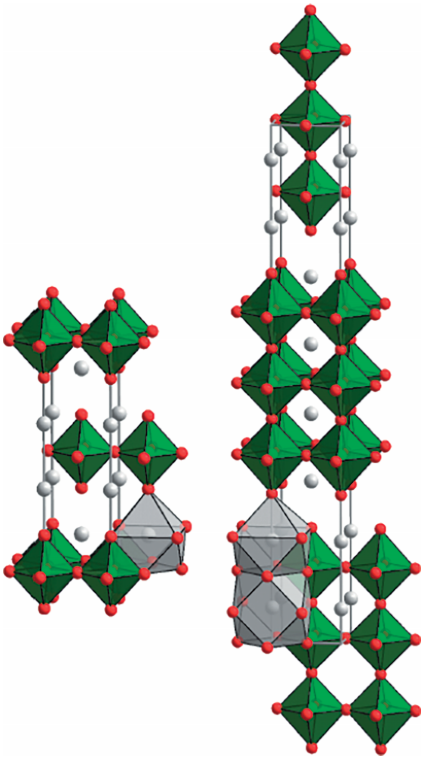

Figure 4. Crystal structures of Ruddlesden–Popper variants with n = 1 (left) and n = 3 (right). Note that E(15) ions are exclusively nine-fold coordinated in the n = 1 variant, while those ions in the n = 3 variant additionally realize cuboctahedral twelve-fold coordination within the perovskite-type slabs (N: green spheres, E: gray spheres, A/R: red spheres).

layers of vertex-sharing octahedra ($(Ba,Sr)_{4/2}Ba_2O$), while the n = 3 member ($(Ba_{1-x}Sr_x)_{10}N_2O)Bi_4$ is an isotype of $Sr_4Ti_3O_{10}$ containing slabs of three layers of vertex-sharing octahedra further connected via corners. In the resulting perovskite slabs, terminal positions of the octahedra are exclusively occupied by Ba, while all Sr together with further Ba accumulates at the equatorial vertices within the layer planes shared by two octahedra. Such a partial order scheme can be expected from ionic size and space filling reasons.

In the above discussed perovskite derivatives, one O^{2-} ion per formula unit is necessary for charge balance. By introducing one trivalent rare-earth metal ion R^{3+} for one alkaline-earth metal ion A^{2+}, the oxide ion O^{2-} can be replaced by further N^{3-}. The resulting nitrides $(R_{1-x}Ca_{3+x}N_{1-x/3})Bi_2$ with R = La, Ce, Pr again represent Ruddlesden–Popper phases with n = 1, meaning K_2NiF_4 structure type compounds.[30] Here, a partial order of R^{3+} and Ca^{2+} on the two available crystallographic sites is due to the different ionic charges and radii. In the La and Ce compounds some excess Ca^{2+} substitutes for R^{3+}, leading to a corresponding small nitride deficiency. Only $(PrCa_3N)Bi_2$ was obtained with ideal composition. All three phases represent heavily doped semiconductors according to electrical resistivity data.

2.2. Inverse Perovskite Nitrides with Group 14 Elements: $(A_3N)E$(14)

Nitrides of the composition $(Ca_3N)E$(14) with E(14) = Ge, Sn, Pb were originally reported to represent metallic, undistorted cubic perovskites with rather unusual electronic structure.[11,31] Later it turned out, that a nitrogen deficiency in $(Sr_3N_x)E$ and $(Ba_3N_x)E$ with E = Sn, Pb and x close to 2/3 nearly yields charge balance.[17] The remaining nitride ions may be disordered over the available positions of the crystallographic site, or order in a perovskite superstructure, depending on synthesis and thermal history of the sample. For the strontium compounds, simple $2 \times 2 \times 2$ superstructures with alternating octahedra fully and partially occupied by N were encountered, basically representing an Elpasolite-type arrangement as given in Figure 5.[17] Independent from possible nitrogen order or exact nitrogen content, the compounds are intrinsically diamagnetic metals, both according to experimental data and electronic structure calculations.

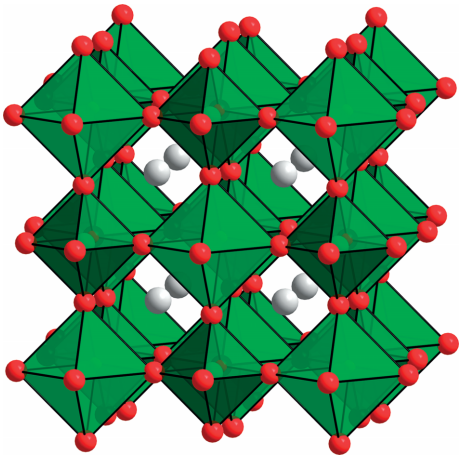

Figure 5. Elpasolite-type order of N in $(Sr_3N_{2/3})E$(14): smaller dark-green octahedra are fully occupied by N, while larger light-green octahedra are occupied to about 1/3 (Sr: red spheres, E: gray spheres).

Upon substitution of 1/3 of the alkaline-earth metal by Eu in $(Ca_2EuN_x)Sn$, a rather unusual case of a homogeneously mixed-valent $Eu^{2+/3+}$-compound was revealed.[32] In the cubic perovskite, nitrogen deficiency with no indication for (partial) order according to powder X-ray diffraction and disorder of Ca and Eu over the respective crystallographic site are present. Furthermore, the Eu atoms coexist in both the +2 and the +3 valence state within the semiconducting material. Various experimental techniques like X-ray absorption and Mößbauer spectroscopy, magnetic susceptibility measurements and chemical analyses result in a formulation summarized according to $Ca_2(Eu^{2+})_{0.75}(Eu^{3+})_{0.25}N_{0.75}Sn$, which represents a charge balanced composition in a simple ionic picture based on exclusively close shell ions Ca^{2+}, N^{3-} and Sn^{4-}.

2.3. Inverse Perovskite Nitrides with Group 13 Elements: $(Ca_3N)E$(13)

Cubic $(Ca_3N)Tl$ is currently the only known example for an alkaline-earth metal (anti)perovskite nitride of group 13 elements, although indications for the possible formation of $(Ca_3N)In$ were obtained.[33,34] The electron deficient compound, in the sense of the ionic limit $(Ca^{2+})_3(N^{3-})(Tl^{3-})$, presents metallic

both according to magnetic susceptibility measurements and electronic structure calculations.[33,35]

2.4. Inverse Perovskite Nitrides with Group 11 Elements: $(Ca_3N)Au$

The metallic cubic perovskite $(Ca_3N)Au$ may be formally written according to $(Ca^{2+})_3(N^{3-})(Au^-)\cdot 2e^-$;[36] however, the itinerant electrons may be accounted to obscure the true electronic nature. The metallic properties result from a broad band formed from Au(6*p*)- and Ca-states near the *Fermi* level, while low-lying states of gold and nitrogen justify the above formulation in the ionic limit.[36,37]

3. Inverse Perovskite Nitrides of the Rare-Earth Metals

Generally, only comparably few ternary nitrides of the rare-earth metals *R* = Sc, Y, La – Lu are known, partly due to the high thermal and thermodynamic stability of the respective binary rare-earth metal nitrides coupled with slow diffusion rates. Perovskites $(R_3Z_x)E$ with *R* = rare-earth metal, *E* = main group metal and *Z* = B, C, N, O (among others) frequently are encountered as impurity phases in entirely intermetallic compounds. Because carbon can be easily added as solid component, while it is more difficult to specifically introduce certain amounts of N and O, many investigations focused on the respective carbides.[38]

In literature the unit cell dimensions of binary intermetallics R_3E and perovskites with C, N, O show significant scatter, however, as a rule for a given rare-earth metal, the values of the carbides are the largest followed by those of the nitrides, oxides and the binary compounds. Deviations from this rule for the perovskites sometimes indicate less than full occupancy of the non-metal site [i.e. $(R_3Z_x)E$ with $x < 1$], while for the binary intermetallic Cu_3Au-type compounds unintended stabilization as perovskites appear rather prevalent (frequently, the reported volumes even exceed those of the corresponding nitride). Additionally, mutual substitution of some rare-earth metal and a metalloid *E* is discussed.[39]

3.1. Inverse Perovskite Nitrides with Indium: $(R_3N)In$

Little experimental information about ternary nitrides with the composition $(R_3N)In$ (*R* = rare-earth metal) is available,[39–42] but a number of studies elucidate various aspects from electronic structure calculations.[40,43–48] The binary compounds $(R_3\square)In$ ($\square$ = vacancy, cubic Cu_3Au structure type) are only known for the larger rare-earth metals, such as *R* = La, Ce, Pr, Nd, Sm, while Sc_3In crystallizes in the hexagonal Mg_3Cd type.[49,50] Due to stabilization by nitrogen the cubic perovskite compounds $(R_3N)In$ were obtained for all rare-earth metals except for yttrium, ytterbium and promethium.[40] For $(Sc_3N)In$ the transition from the hexagonal binary intermetallic compound to the cubic perovskite indicates a structure determining effect of the nitride ion, as discussed in more detail for the reversible case of related perovskite hydrides.[51] All compounds $(R_3N)In$ readily react with excess N_2 at elevated temperatures forming the binary rare-earth metal nitride *R*N and In metal.[52]

Figure 6. shows the unit cell volumes of the perovskite nitrides depending on the radius of the trivalent rare-earth metal ions in six-fold coordination.[53] A close inspection of these values reveals $(Ce_3N)In$ to smoothly fit into the trend of most other rare-earth metal perovskite nitrides indicating the presence of Ce^{3+}, while the unit cell of $(Eu_3N)In$ deviates to considerably larger values, revealing contributions by Eu^{2+}, as was similarly found for $(Eu_3O)In$.[54]

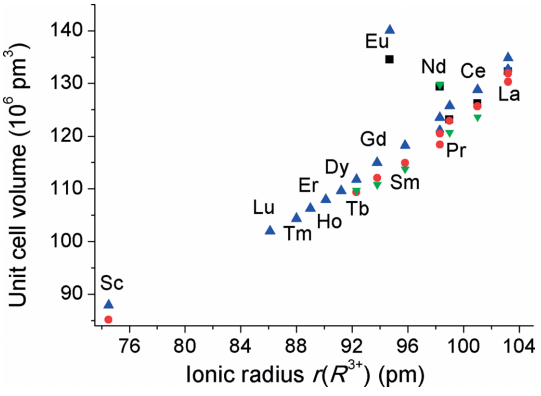

Figure 6. Unit cell volumes of rare-earth metal perovskite nitrides $(R_3N)E$ (*E* = In: blue triangles, Ga: green triangles, Al: red circles, Sn: black squares) depending on ionic radius of the respective rare-earth metal ion in trivalent state and with coordination number of 6 . For references compare main text body.

All compounds $(R_3N)In$ are metallic, with the magnetic properties dominated by the rare-earth metal ions.[55] While La_3In shows a superconducting transition at $T_c \approx 10$ K,[56] $(La_3N)In$ lacks any indication for superconductivity. Earlier it was observed that T_c does not significantly change with introduction of O or B into La_3In within the full range of $0 \le x \le 1$ in cubic $(La_3Z_x)In$, while T_c decreases continuously upon addition of carbon.[41] At lower temperatures the compounds $(R_3N)In$ with *R* = Ce, Pr, Nd, Tb order antiferromagnetically at T_N = 9.0 K, 10.8 K, 8.8 K, and 30 K, respectively, while the low-temperature susceptibility of $(Sm_3N)In$ is modified by the presence of exited states, but also shows indications for an antiferromagnetic order.

The commensurate zero-field magnetic structure of $(Ce_3N)In$ was determined from powder neutron diffraction.[42] The magnetic ordering can be represented with three antiferromagnetic substructures with magnetic components localized on Ce^{3+} ions orientated parallel to the orthogonal crystallographic axes. High-field magnetic susceptibility measurements reveal multi-step metamagnetic behavior with different numbers of steps for $(Ce_3N)In$, $(Pr_3N)In$ and $(Nd_3N)In$.[55]

3.2. Inverse Perovskite Nitrides with Aluminium: $(R_3N)Al$

In the binary systems *R*–Al phases with the composition R_3Al were reported for *R* = Y, La–Nd, Sm, Tb–Er to realize a hexagonal Ni_3Sn type structure.[57–61] Phases crystallizing in the Cu_3Au crystal structure frequently observed in literature are likely to

be stabilized by unnoticed C, N, O impurities,[62] since the reported unit cell parameters considerably scatter and direct transformation from the hexagonal to the cubic phase was observed only upon annealing in quartz ampoules or MgO crucibles.[63,64]

Several cubic perovskite nitrides with aluminium were reported with *R* = Sc, La–Nd, Sm, Gd, Tb.[34,39,55,65,66] Interestingly, no respective yttrium perovskite nitride of Al was obtained.[67] These aluminum compounds show an increased stability against excess nitrogen compared to the respective indium compounds: They directly form upon heating of the metallic elements in nitrogen gas and produce mixtures of rare-earth metal and aluminum nitrides only at significant higher temperatures. Additionally, they seem to tolerate only minute deficiencies of nitrogen.[68]

Figure 6 plots the unit cell volumes for the compounds (R_3N)Al as a function of the ionic radii of the rare-earth metal ions in the oxidation state +3 (*CN* = 6),[53] giving a rather smooth dependence without any significant deviation, particularly not for (Ce_3N)Al already indicating an exclusive trivalent state of Ce. Magnetic susceptibility measurements on (Ce_3N)Al clearly indicate an Ce($4f^1$) electronic state ($^2F_{5/2}$ crystal field ground multiplet). (Ce_3N)Al below 6 K orders antiferromagnetically, at temperatures well below T_N it shows a multi-step metamagnetic behavior.[55,68]

3.3. Inverse Perovskite Nitrides with Tin: (R_3N)Sn

In the binary systems *R*–Sn phases R_3Sn were reported for *R* = La, Ce, Pr to crystallize in the Cu_3Au structure type.[69] Particularly La_3Sn received some attention, since it shows superconductivity up to 6.2 K,[70] but does not appear in any phase diagram. As frequent, the reports on such a cubic binary intermetallic phase may be due to unnoticed impurities of light elements like C, N, or O. The perovskite nitrides of La, Ce, Nd, Pr, and Sm were reported and apparently also (Eu_3N)Sn can be produced,[34,55,71] but the uncertainty in valences complicates single phase synthesis of the europium compound as discussed for (Ca_2EuN_x)Sn constituting from mixed-valent $Eu^{2+/3+}$ (see paragraph 2.2).[32]

Figure 6 plots the volumes of the compounds (R_3N)Sn as a function of the ionic radii of the rare-earth metal ions in the oxidation state +3 (*CN* = 6).[53] The values are well in correspondence with each other, only the reported volume of (Nd_3N)Sn from an independent study strongly deviates towards a larger value.[39,71] Particularly the volume of (Ce_3N)Sn does not deviate to lower values, indicating a pure Ce^{3+} state for the nitride.

Metallic (La_3N)Sn shows a weak, nearly temperature independent paramagnetism in the expected range for Pauli-paramagnetism.[71] A transition to superconductivity at T_c = 5.8 K probably is due to minor impurities of β-La. (Ce_3N)Sn and (Pr_3N)Sn are Curie–Weiss paramagnets, in full agreement with an exclusive presence of both rare-earth metals in the trivalent valence state, showing antiferromagnetic order below 6.8 K and 48 K, respectively.[71] For (Ce_3N)Sn at lower temperatures a metamagnetic transition starting above an external magnetic field of 32 kOe is observed, during which the antiferromagnetic spin arrangement changes reversibly to a spin state with higher magnetization.

3.4. Inverse Perovskite Nitrides with Gallium, Thallium and Lead: (R_3N)*E*

For all three systems in an early publication the respective neodymium compounds, (Nd_3N)Ga, (Nd_3N)Tl and (Nd_3N)Pb were reported.[39] The presence of further cubic perovskite nitrides with these main group elements was indicated and particularly for *E* = Ga confirmed. Figure 6 contains the volumes of the cubic perovskites (R_3N)Ga with *R* = Ce, Pr, Nd, Sm, Gd, Tb.[34,39,55] Remarkable, the volumes of these gallium compounds are smaller than those of the respective aluminium compounds, supporting the anionic nature of these metal atoms, since gallide ions are generally smaller than equally charged aluminide ions, despite the larger atomic and cationic radii of gallium.[72]

4. Inverse Perovskite Nitrides of the Transition Metals

4.1. Binary Inverse Perovskite Nitrides of the Transition Metals: M_4N

Few binary nitrides of the transition metals crystallize in the perovskite structure. Prototype is the cubic γ′-Fe_4N, also occurring in nature as rare meteorite mineral Roaldite,[73] with the iron atoms realizing the motif of a cubic closed (*fcc*) packing and nitrogen located in one quarter of the octahedral holes in an ordered manner, such that they are exclusively corner-sharing. Three iron atoms per formula unit are thus linearly coordinated by N and one iron atom solely surrounded by twelve Fe of the other kind within a cuboctahedron (see Figure 7). Thus,

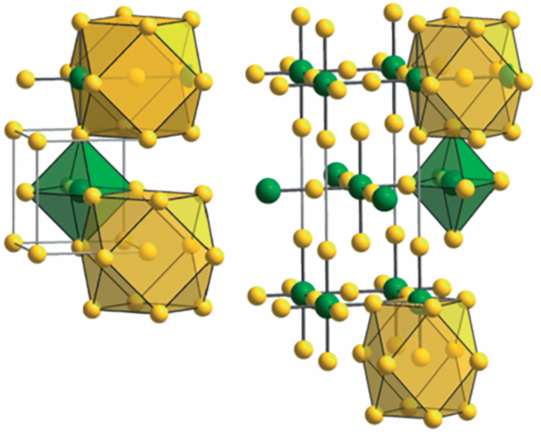

Figure 7. Crystal structures of γ′-Fe_4N (left) and the most stable modification of Ni_4N (right). Note the similarities of both structures based on the motif of a *fcc* packing of the transition metal atoms (yellow) with different order patterns of occupation of one quarter of the octahedral holes by N (green). In this way, all transition metal atoms are mutually cuboctahedrally coordinated. In the γ′-Fe_4N-type, three quarter of the Fe are linearly coordinated by N, while one quarter has no N in close proximity. In Ni_4N, in contrast, only one half of the Ni atoms are linearly coordinated, whilst the other half has one contact to N (adapted from ref.[87]).

this composition may alternatively written according to $(Fe_3N)Fe$. Next to other binary iron nitrides, this phase is well-established for various technical applications, for example, in the industrial surface hardening of steel work pieces, improving hardness and tribological properties as well as corrosion and wear resistance.[74] Owing to its ferromagnetic properties up to about 770 K,[75] which are tunable in large ranges via substitution, it gained interest in magnetic data recording.[76,77] According to the accepted binary phase diagram γ′-Fe_4N shows only a narrow homogeneity width within the whole range of existence up to 953 K.[78] Polycrystalline γ′-Fe_4N transforms into single crystalline hexagonal ε-$Fe_3N_{0.75}$ under high-pressure high-temperature conditions (8.5 GPa and 1373 K) and reforms upon heating after release of pressure.[79]

ε-Mn_4N, Co_4N, Ni_4N and Cu_4N were reported to crystallize in the γ′-Fe_4N type structure but are less well studied. ε-Mn_4N with a Curie temperature of about 756 K and a non-collinear ferrimagnetic spin-structure exists with a rather small homogeneity range, attributed to Frenkel type disorder of nitride ions.[80–82]

Co_4N is ferromagnetically ordered up to the decomposition starting above 630 K, with a magnetic moment higher than the one for pure Co.[83] It recently gained interest as catalytic material for several applications like, for example, decomposition of hydrazine, reduction of nitrogen monoxide, oxidation of carbon monoxide, hydrodenitrogenation of crude oil and water splitting.[84]

For Ni_4N two forms differing in the nitrogen order within the Ni-*fcc* motif were reported as compared in Figure 7, one with the cubic γ′-Fe_4N-type structure and one with a tetragonal two-dimensional sheer structure of the first, now with half of the Ni coordinated linearly by N and the other half by only one N.[85] Electronic structure calculations revealed a lower energy for the second form, but both to be metastable against decomposition into Ni and Ni_3N.[86,87] Ni_4N orders ferromagnetically.[86]

Synthesis of the perovskite Cu_4N was reported only once, obtained as a thin film by plasma deposition.[88] However, electronic structure calculations failed to reproduce the experimental unit cell and revealed its metastable nature against decomposition into the elements, which is not necessarily a contradiction.[86]

4.2. Ternary and Multinary Inverse Perovskite Nitrides of the Transition Metals: $M_{4-x}M'_xN$

As already mentioned, the γ′-Fe_4N structure type consists of three Fe atoms per formula unit coordinated by N and one Fe atom entirely surrounded by a cuboctahedron of twelve Fe of the first kind and no N in its first coordination sphere. Both metal sites are susceptible to substitution by other metals. Within such substituted ternary variants, a more nitrophilic (less electronegative) element typically occupies the position with N in close proximity, while the exclusively by metal atoms coordinated position typically accumulates less nitrophilic (more electronegative) metals, which themselves do often even not form any stable binary nitrides. Such ternary perovskite nitrides with general formula $M_{4-x}M'_xN$ can tolerate the whole range of $0 \le x \le 4$ with disorder of the metallic components, if their interactions with nitrogen as well as mutual bonding are sufficiently similar. If the interaction of the metallic constituents with nitrogen is rather different, particularly in case of more electronegative metalloids as component *M′*, the latter atoms avoid nitrogen and a maximum substitution of typically $x \le 1$ results, i.e. compositions $(M_3N)M'$ directly interlinking to the above discussed alkaline-earth and rare-earth metal compounds. Structural distortions to various tetragonal variants are most frequently observed for manganese-based perovskites with main-group elements, but also encountered for such iron- and chromium-based compounds and Mn_3CuN (see below).

Ternary transition metal perovskite nitrides were initially primarily studied for their magnetic properties, recently interest re-aroused due to various relevant properties affiliated with specific element combinations.

4.2.1. Ternary and Multinary Iron-Based Inverse Perovskite Nitrides: $Fe_{4-x}M_xN$

γ′-Fe_4N as the binary prototype for this group of compounds is especially prone for substitution of iron by a large variety of different metals. The substitution $Fe_{4-x}M_xN$ can principally occur on both metal sites, depending on the nature of *M*. The full range of $0 \le x \le 4$ is particularly accessible for metals that form γ′-M_4N phases themselves, while less nitrophilic elements with larger electronegativity like the main group metametals and the noble metals rather substitute on the metal site exclusively coordinated by further metal (Fe) atoms. The latter results in a maximum substitution of $x = 1$ eventually leading to ordered compounds Fe_3MN. Upon substitution the resulting phases either remain ferromagnetic modifying the properties of γ′-Fe_4N – this case mostly encountered with *M* being a transition metal – or develop a frustrated magnetic spin system – frequently found in case of iron substitution by a main group element.

Reports on synthesis of $Fe_{3-x}Co_xN$ in bulk are rare.[89,90] Mößbauer spectroscopy and XMCD on thin films as well as Mößbauer on bulk samples with $x < 1$ indicate complete disorder of the metallic constituents.[91] In agreement, electronic structure calculations reveal positive formation energies for the composition Fe_3CoN. Disorder is easily rationalized by the alike chemical behavior of iron and cobalt together with very similar atomic radii, although indications for a minute preference of Co avoiding nitrogen in direct neighborhood for this composition was obtained in an independent study.[92,93] A fully ordered variant of Fe_3CoN was predicted to exhibit a ferromagnetic ground state with a total magnetic moment similar to the value for γ′-Fe_4N.[94,95] The more cobalt-rich disordered phase $FeCo_3N$ orders ferromagnetically according to XMCD measurements,[91] while the (hypothetical) ordered compound with this composition was predicted to represent a half-metal with a band gap of 0.2 eV at the Fermi level and thus possess potential for spintronic applications.[96]

Substitution phases with Ni are stable compounds in the whole composition range of $Fe_{4-x}Ni_xN$, although Ni_4N (i.e. $x = 4$) realizes a different structural ground state variant (see above and Figure 7).[97–99] Literature provides a large number of studies of various kinds, which are beyond the scope of this review.

The substitution of Fe by Ni tends to reduce the unit cell dimensions and thermodynamic stability of the compounds as well as the magnetic moment and the Curie temperature.[97,100,101] Preference of Ni on the metal site with no direct contact to N was deduced from Mößbauer and X-ray absorption spectroscopy, and X-ray magnetic circular dichroism.[75,90,102] For fully ordered Fe_3NiN coexistence of localized moments at Ni and itinerant moments for the Fe atoms were predicted by electronic structure calculations.[103] Highly (100) orientated Fe_3NiN thin films on sapphire substrate presented ferromagnetic with square-shaped hysteresis and were proposed for spintronic devices and magnetic sensors.[98] For thin films with overall composition of Fe_2Ni_2N and thickness in the order of 40 nm fabricated by molecular beam epitaxy an observed tetragonal distortion of the cubic structure may suggest order within layers parallel to (100).[104]

$Fe_{4-x}Mn_xN$ bulk samples were obtained with x up to 1.[105] Mößbauer spectroscopy indicated random arrangement of iron and manganese over both sites, possibly with little preference of Mn for the site distant to N, which was associated with the similar radii of both metals in agreement with an only slightly larger cubic unit cell of the binary manganese nitride as compared to γ′-Fe_4N. Improvement of magnetic properties, particularly the remanence and the coercive field with manganese substitution was discussed as advantageous for magnetic recording. Thin films with x in the full substitutional range were fabricated in order to study the transport properties of the materials.[106] Electronic structure calculations reveal some competing anti-ferromagnetic and ferrimagnetic behavior dependent on the site substituted by Mn.[107,108]

Only few experimental studies on the substitution of γ′-Fe_4N with the coin metals Cu, Ag, Au were reported. Thin films incorporating only small amounts of copper were presented.[109,110] In bulk, for copper and silver only maximal substitution of x = 0.5 and x = 0.36, respectively, was obtained after mechanical alloying with subsequent annealing, while with gold a composition of Fe_3AuN was reached.[110,111] Although Mößbauer spectroscopy revealed that these substitutes rather occupy the site with no nitrogen in its coordination due to significant stronger attractive interactions between iron and nitrogen, the order of the resulting phases was probably incomplete. Recently, $Fe_{3-x}Cu_xN$ gained interest as soft magnetic material due to several favorable properties as increased permeability and reduced power loss.[112]

$Fe_{3-x}Zn_xN$ with x = 0.6 was obtained by mechanical alloying.[113] Apparently, the Zn only fully orders to occupy the distant to N site in the structure upon annealing after ball milling, both according to magnetic and Mößbauer data. The synthesis of a higher substituted sample with x = 1, however, was questioned.[114]

Apparently, there is only one experimental report on phases with M = Ru, Os substituting iron in γ′-Fe_4N in literature.[115] Samples with up to x = 0.2 in $Fe_{3-x}M_xN$ were synthesized and Mößbauer spectroscopy indicated occupation of the exclusively by iron coordinated site by M. Ferromagnetic ground states were predicted by a number of theoretical studies, focusing on fully ordered compounds Fe_3MN.[116] A rather limited substitution by these elements was later rationalized by total energy electronic structure calculations, indicating significant positive formation energies.[92] Very similar is true for M = Ir, where the experimental knowledge is even further limited,[115] and electronic structure calculations indicate a ferromagnetic ground state for the to date still hypothetical fully ordered compound Fe_3IrN, which should be stable at elevated pressures.[92,95,117] In contrast, Fe_3RhN represents a fully ordered stable ferromagnetic compound, both from experiment and theoretical considerations.[92,95,118] Few experimental studies address the systems $Fe_{4-x}M_xN$ with M = Pd, Pt, giving clear evidence of the presence of fully ordered compounds Fe_3PdN and Fe_3PtN as the end members,[119] in well agreement with the prediction as stable compounds.[92] According to electronic structure calculations, both are foreseen to possess ferromagnetic ground states.[103,108,119]

Main group semimetals apparently also rather avoid direct contact to nitrogen upon partial substitution of iron, naturally resulting in Fe_3MN as the compounds with maximal degree of substitution. Although some authors claim a somewhat higher substitution of iron by tin up to x = 1.2 in $Fe_{4-x}Sn_xN$ and possible occupation of both iron sites,[120] most and especially the newer studies indicate a clear site preference.[121] Interestingly, for this particularly well studied system a small miscibility gap around x = 0.33 was indicated. Generally, the ferromagnetic interactions are weakened with increasing substitution by tin and approaching x = 0.9 a spin glass with frustrated spin ground state develops due to competing interactions.[122]

Fe_3GeN_{1-y} realizes a slight distortion from cubic perovskite structure towards tetragonal, while solid solutions $Fe_{4-x}Ge_xN_{1-y}$ with x < 1 rather remain cubic.[123–126] In the tetragonal structure every second layer of octahedra parallel to (001) are rotated in opposite directions (space group *I*4/*mcm*, see Figure 8). This variant of tetrahedral distortion in literature frequently is denoted T4 or characterized as stuffed USi_3-type structure. In the resulting structure of Fe_3GeN_{1-y} the octahedra around N are stretched along the tetragonal [001] direction by about 3 % and the angle N–Fe–N within (001) result to about 170° due to the octahedra kinking. Nitrogen content for cubic phases decreases with increasing germanium content, however, restores to a cer-

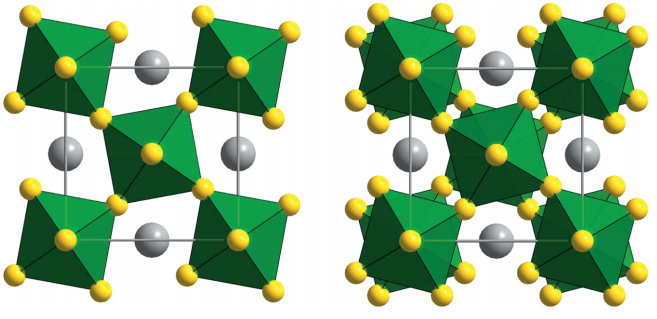

Figure 8. Crystal structures of tetragonal distorted perovskites in T2 (space group $P\bar{4}2_1m$ and enlarged unit cell by $a' = a\sqrt{2}$ and $c' = c$ relative to the cubic unit cell, left) and T4 (*I*4/*mcm* with $a' = a\sqrt{2}$ and $c' = 2c$, right), transition metal atoms (yellow), N (green). Note that surrounding of cuboctahedrally coordinated metalloid atoms (gray) become increasingly distorted upon symmetry reduction.

tain amount upon tetragonal distortion. Ferromagnetic interactions decrease with increasing Ge content, until the frustrated state turns to paramagnetic at 76 K.[125] The co-substituted series $Fe_3Ge_{1-x}Sn_xN$ interesting remains cubic over the whole range of composition and retains high nitrogen contents close to unity.[127]

Increasing substitution with Ga in cubic $Fe_{4-x}Ga_xN$ leads to a gradual transformation from ferro- to antiferromagnetic order upon approaching the limit of x slightly below unity.[128,129] $Fe_{4-x}In_xN$ exists fully ordered up to at least $x = 0.8$ as a cubic ferromagnet.[130] However, a sample obtained via mechanical alloying was found to show some Fe/In disorder and an indium content of up to $x = 1$.[113] In strong contrast Fe_3AlN was reported several times, but recently questioned, since obtained samples were shown to rather consist of an intimate mixture of γ′-Fe_4N and amorphous aluminium oxide.[114,129,131]

4.2.2. Ternary and Multinary Manganese-Based Inverse Perovskite Nitrides: $Mn_{4-x}M'_xN$

Recently, multinary Mn_4N-based perovskite nitrides gained considerable interest, namely $Mn_3Cu_{1-x}(Ga,Si,Ge,Sn,Ag)_xN$, $Mn_3(Zn,Sn)N$ and related compositions, due to their tunable near zero to largely negative isotropic thermal expansion originating in a magnetovolume effect.[132] Still, surprisingly little is known about some of the respective single substituted phases. An early study, for example, deduced a maximum x of 0.65 for $Mn_{4-x}Cr_xN_{1-y}$ and 0.56 for $Mn_{4-x}Fe_xN_{1-y}$, respectively, and argued for a preferred Cr substitution on the sites with N in direct contact, solely based on higher thermal stability of chromium nitrides compared to manganese nitrides, while Fe was expected to occupy both positions.[133] Cubic Mn_3CoN_{1-y} is reported to show antiferrimagnetism below $T_N = 252$ K.[134] For Mn_3NiN, in contrast, magnetic structures across the Néel temperature with fully compensated antiferromagnetic order at lower temperatures and canted variants allowing for some ferromagnetic components were reported quite early.[135] A large negative thermal expansion below the Néel temperature of 264 K results from magnetostriction during a continuous spin rearrangement, which might be controlled by the degree of substitution in $Mn_{4-x}Ni_xN$.[136] Additionally, a magneto-mechanical coupling results in an abnormal large piezomagnetic effect.[137] Mn_3RhN and Mn_3PdN also realize antiferromagnetic order below about 226 K and 316 K.[134,138] While Mn_3PtN, like the two aforementioned noble metal compounds, remains cubic, with reduced nitrogen content $Mn_3PtN_{0.25}$ and $Mn_3RhN_{0.2}$ crystallize in a hexagonal 2H-perovskite structure ($BaNiO_3$-type structure, see Figure 3).[139]

Upon cooling, cubic Mn_3ZnN changes from a Curie paramagnet to an antiferromagnet below about 180 K, with a magnetic rearrangement at 127.5 K.[134,140] Interestingly, in a temperature interval of 140 K – 177 K two different magnetic structures were observed to coexist.[141] Mn_3AgN is a triangular antiferromagnet with weak ferromagnetic contributions below 366 K and transition to a non-coplanar ferromagnetic state below 15 K.[134,142] Mn_3CuN orders ferrimagnetically below about 143 K, concomitant to a distortion to tetragonal metric due to magnetostriction.[143] The observed distortion with a ratio $c/a < 1$ is often denoted T_1^- in literature. Little is known about cubic Mn_3AuN and Mn_3HgN (including the phase $Mn_{4-x}Hg_xN$).[138,144]

With main group element substitution, cubic Mn_3GaN is probably the best investigated manganese-based perovskite nitride. Upon decreasing temperature, a transition from Curie paramagnetic to antiferromagnetic order was observed at about 290 K followed by a reentrance spin-glass state below 133 K. Furthermore, with additional Ge-substitution, a large negative thermal expansion coefficient close to room temperature was revealed.[134,140,145–147] Comparably little is known about Mn_3AlN_x, which was reported to exhibit a very high Curie temperature of up to 818 K.[148] Mn_3InN apparently was only studied once experimentally, revealing antiferromagnetism below room temperature.[149] A decreasing Curie temperature and magnetic moment of $Mn_{4-x}In_xN$ upon increasing substitution by In was reported earlier.[150]

A tetragonal distortion to a T_4 type structure (space group $I4/mcm$) was reported for Mn_3GeN_x (compare Figure 8).[123,134,151,152] In cubic $Mn_{4-x}Sn_xN$ the magnetic moment as well as the Curie temperature drops with increasing substitution.[138,150] For $Mn_{3.1}Sn_{0.9}N$, a ferromagnetic component in the temperature range of 5–370 K and a spin-reorientation at about 280 K was described.[153]

Mn_3SbN undergoes a first order transition from Curie paramagnetic to ferrimagnetic order, concomitant to a distortion to tetragonal metric at 360 K due to large magnetostriction, resulting in a ratio $c/a > 1$, typically termed T_1^+ Mn_3AsN in contrast rather distorts differently due to rotation of the octahedral, resulting in the T_4 type (see Figure 8).[134,151,154–156]

4.2.3. Ternary and Multinary Nickel-Based Inverse Perovskite Nitrides: $Ni_{4-x}M'_xN$

Research in Ni-based perovskites was triggered by the discovery of superconductivity in Ni_3MgC with a transition temperature of 8 K in 2001, leading to the finding of type II superconductivity in cubic Ni_3CuN and Ni_3ZnN with T_c around 3 K.[157] For Ni-rich perovskite nitrides with iron see the comments in paragraph 4.2.1. Cubic Ni_3CdN was reported to exhibit paramagnetism or very soft and weak ferromagnetism, and forms a solid solution with cubic and ferromagnetic Co_3CdN in the full range of compositions.[158] Fully ordered cubic Ni_3InN shows spin-glass-like behavior.[159,160]

4.2.4. Ternary and Multinary Cobalt-Based Inverse Perovskite Nitrides: $Co_{4-x}M'_xN$

The knowledge on cobalt-based perovskite nitrides appears limited. Apparently, compounds with Zn and Mg form in addition to the cubic ferromagnet Co_3CdN and its solid solution with Ni_3CdN.[131,158a] Recently, cubic Co_3SnN was synthesized after prediction of its stability via a high-throughput screening by DFT methods.[161,162] Cubic Co_3InN and Co_3GeN show spin-glass behavior, probably as a result of minor disorder or – more likely – main-group metal vacancies.[153,160,163] For Co-rich perovskite nitrides with iron see the comments in paragraph 4.2.1.

4.2.5. Ternary and Multinary Copper-Based Inverse Perovskite Nitrides: $Cu_3M'_xN$ and $Cu_{4-x}M'_xN$

The situation in the copper-rich systems is different from the other transition metal phases, since Cu_3N exists with ReO_3-type

structure as a semiconducting and rather covalent compound. It can host further metals in the large resulting void, leading to cubic perovskites. Particularly Cu_3Pd_xN with $x = 0.020$ and 0.989 were characterized to show a semiconducting-to-semimetallic transition with increasing x, eventually leading to a Dirac semimetal.[164,165] Thin films with $x = 0.238$ exhibit a vanishing temperature coefficient of the electrical resistivity, due to a delicate balance of carrier concentration and mobility.[166] A similar situation was observed for thin films Cu_3M_xN with M = Cu, Ag, Au, while for nanocrystalline Cu_3Zn_xN films only small x were obtained.[167] Still, the Zn intercalation provokes a rapid drop of electrical resistivity. A narrow-gap semiconductor $Cu_3Au_{0.5}N$ was additionally reported.[168]

In contrast, upon lithium intercalation into Cu_3N, copper is partially replaced by Li, and enters the site not coordinated to N in the resulting perovskite Cu_3Li_xN ($0 < x \leq 1$).[169] Similarly in thin films, Ni in a lower concentration substitutes Cu in Cu_3N, before it eventually enters the vacant site.[170]

4.2.6. Ternary and Multinary Chromium-Based Inverse Perovskite Nitrides: $Cr_{4-x}M'_xN$

Little information on Cr-based ternary perovskite nitrides is available, although interest is currently reawakening. Cubic Cr_3PtN was studied as precipitate and protective layer upon nitridation of Cr_3Pt and Pt containing chromium alloy, while cubic Cr_3PdN gained interest due to a magnetic spin-glass behavior, whose origin was traced back to disordered vacancies in the nitrogen substructure confirmed by complementary investigation of $Cr_3PdN_{0.75}$.[152,171,172] Cr_3IrN and Cr_3RhN apparently were only once synthesized, while several studies predict superconductivity in Cr_3RhN at comparably high temperatures in the order of 17 K.[152,173,174]

Similarly, only synthesis and unit cell of cubic Cr_3SnN was reported so far.[152] Cr_3GaN also crystallizes as cubic perovskite and was predicted to become superconducting below some 4 K.[152,173,175–177] The $Cr_{6/2}N$ octahedra in Cr_3GeN and Cr_3AsN are subject to rotation, resulting in tetragonal distorted variants T2 and T4, respectively (compare Figure 8).[123,152,178] Upon heating of Cr_3GeN a series of transitions from T2 to T4 and a higher symmetric tetragonal phase very similar to T2 to eventually reach cubic perovskite structure was revealed.[179] The first structural transition proceeds concomitant to loss of antiferromagnetic order with large hysteresis at 150 °C, the cubic phase is stable above 750 °C.[180] A similar magnetic transition with loss of magnetic order was observed for Cr_3AsN, however, not associated with a structural change and at considerably lower temperature around 243 K.[181]

4.2.7. Ternary and Multinary Titanium-Based Inverse Perovskite Nitrides: $Ti_{4-x}M'_xN$

Despite the fact that no binary perovskite nitride of Ti is known, some compounds Ti_3MN were reported. Particularly Ti_3AlN was recently studied in-depth due to its outstanding hardness and abrasive properties.[182] However, with the related compounds Ti_3InN and Ti_3TlN and phases $Ti_3(M_{1-x}Ti_x)N_y$ exhibiting some Ti excess [$Ti_{3.1}Zn_{0.9}N_{0.5}$, $Ti_{3.2}Zn_{0.8}N_{0.8}$, Ti_3(Ti,Cd)N, $Ti_{3.2}Hg_{0.8}N$] only few further examples for such perovskites were described and hardly anything more than the cubic unit cell is known.[176,183]

4.2.8. Ternary and Multinary Inverse Perovskite Nitrides Based on Further Transition Metals: $M_{4-x}M'_xN$

The formation of a cubic phase with composition V_3AuN_x was observed.[184] Furthermore, a hexagonal perovskite Re_3ZnN_x with 4H-$BaRuO_3$ type structure (compare Figure 3) was described.[185]

5. Synthetic Considerations

Synthesis of ternary perovskite nitrides under discussion crucially depends on the element combination in the desired product. The alkaline-earth metal compounds of paragraph 2 mostly form directly from the metallic components in presence of excess nitrogen leading to stable compounds.[26] Crystal growth succeeded starting from strontium nitride in a flux of molten lithium for several examples, while crystals of $(Ca_3N)Tl$ were obtained from excess calcium above its melting point.[17,33] The rare-earth metal compounds of paragraph 3 in contrast at elevated temperatures typically are unstable against further nitridation to form the binary rare-earth metal nitrides next to the element, binary intermetallic or binary nitride of the second component, depending on its nitrophilicity and affinity to form binary compounds with the rare-earth metal.[52,55] In such systems, the nitrogen frequently readily substitutes with oxygen or carbon, for example, and nitrogen deficiencies may occur. Thus, synthesis of single phase material is often hindered and requires highly pure substances and gases, exact stoichiometric ratios of all starting materials including the anticipated nitrogen content as well as fully inert crucibles.[32,54,68,71] Few examples of crystal growth for these compounds can be found in literature, mostly as result of elevated temperatures, possibly aided by self-flux of the metallic components during formation of the final perovskite material.[54,55,68]

Transition metal-based perovskite-nitrides in contrast typically do not take up any oxygen into the nitride phase, although undesired oxidation may occur at surfaces and grain boundaries. Synthetic challenges in these systems rather concern the single phase synthesis, the sometimes variable nitrogen content and unintended substitution with magnetic impurities, which may significantly alter the magnetic properties of the obtained materials. In order to overcome obstacles from diffusion several approaches were developed, for example mechanical alloying of metals with binary nitrides or of purely the metallic constituents with subsequent annealing in nitrogen or ammonia.[105,109–111,113,118a] This approach typically arrives at small particle sizes, depending on system and annealing temperature, which can be interesting from nano-chemistry and -magnetism or an enlarged surface point of view, but the products often are difficult to characterize with respect to composition, impurities, crystal structure details and so on. Alternatives employ mixtures of oxides and metals, mixed-transition metal oxalates or even sol-gel-techniques, for example via the citrate route, for atomic-level intermixture of metallic components prior to ammonolysis.[90,97,99,101,105,112] Recently, Ni_3ZnN, Co_3SnN and their analogous carbides were synthesized from reactions of their corresponding oxide mixtures with gaseous decomposition products of melamine.[161] The nitrides within

this technique form at lower temperatures than the carbides. However, no clear evidence for formation of pure nitrides or carbides was presented.

One elaborate technique used coprecipitation of hydroxides followed by reduction in hydrogen and subsequent nitridation in hydrogen/ammonia mixtures in a fluidized-bed reactor.[115] More general, a two-step synthesis with a high-temperature period aiding interdiffusion of metallic components and reduction, followed by a lower-temperature nitridation step gives improved results, particularly in systems where low thermodynamic stability paves way of binary intermetallic impurity and side-phases.[92,118,129,186] According to the decomposition equilibrium of ammonia to elemental nitrogen and hydrogen,

$$NH_3 \rightleftarrows {}^1/_2\ N_2 + {}^3/_2\ H_2$$

the chemical potential μ(N) of nitrogen can be adjusted by the ratio of ammonia and hydrogen in a gas mixture

$$\boldsymbol{\mu}(\mathrm{N}) = \boldsymbol{G}^{\circ}(\mathrm{NH_3}) - \boldsymbol{G}^{\circ}(\mathrm{H_2}) + \boldsymbol{RT}\ \mathbf{ln}\frac{\boldsymbol{p}(\mathrm{NH_3})}{\boldsymbol{p}(\mathrm{H_2})^{3/2}}$$

In the equation above, $\mathbf{ln}\frac{\boldsymbol{p}(\mathrm{NH_3})}{\boldsymbol{p}(\mathrm{H_2})^{3/2}}$ denotes the so-called nitridation potential according to Lehrer.[187] Thus, nitride formation and content in the product can be adjusted by a proper gas mixture depending on nitridation temperature, giving access to even metastable phases.[186]

Recently, we have developed an electrochemical synthesis of transition metal perovskite nitrides (M_3M'N) with a metametal M', typically In or Sn. This approach employs a molten eutectic of LiCl/KCl as electrolyte (melting point 625 K),[188] a small amount of Li_3N as nitrogen reservoir dissolved in the salt melt and a nitrogen gas electrode for nitrogen supply, while an intermetallic melt bead of the constituting metals in the desired atomic ratio is used as working electrode.[160,189,190] Apparent advantages of this technique are the reduced nitridation temperature, so far only limited by the melting point of the inert electrolyte and the resulting high nitrogen content in the products. However, this technique still deserves optimization.

Colloidal Cu_3PdN nanoparticles were obtained from reaction of nitrates and acetylacetonates in organic solvents.[191] Furthermore $Mn_{4-x}Hg_xN$ was obtained from liquid Mn-amalgam with ammonia,[144] and $Mn_{3.07}Ga_{0.93}N$ from Mn and Ga in molten sodium with application of 5 MPa nitrogen pressure.[146] High-pressure synthesis in a belt-type apparatus at 6 GPa and 1250 °C was applied for synthesis of polycrystalline Mn_3InN.[149] Similarly, Re_3ZnN_x was obtained under high-temperature high-pressure conditions in a diamond anvil cell.[185]

Ammonothermal synthesis combines the advantages of solvent, here supercritical ammonia, with elevated pressures above 6 kbar and temperatures of up to 600 °C. Under such conditions, single crystals Cu_3Pd_xN with x = 0.020 and 0.989 were obtained.[164]

Acknowledgments

Special thanks go to my beloved daughter Caroline L. Niewa for translating the original Latin publication of Gustav Rose.

Keywords: Nitrides · Perovskites · Structure variants

[1] G. Rose in *De perowskite, fossili novo*, in *De novis quibusdam fossilibus quae in Montibus Uraliis inveniuntur*, A. G. Schade, Berlin, Germany, **1839**, pp. 3–5.
[2] a) T. Barth, *Norsk. Geol. Tidsskr.* **1925**, *8*, 201–216; b) W. H. Zachariasen, *Norsk. Vidensk. Akad. Oslo, I. Mat. Naturv.* **1928**, *4*, 1–165.
[3] O. Bock, U. Müller, *Acta Crystallogr., Sect. B* **2002**, *58*, 594–606.
[4] a) L. Katz, R. Ward, *Inorg. Chem.* **1964**, *3*, 205–211; b) J. Darriet, M. A. Subramanian, *J. Mater. Chem.* **1995**, *5*, 543–552.
[5] a) V. M. Goldschmidt, *Naturwissenschaften* **1926**, *14*, 477–485; b) V. M. Goldschmidt, in *Geochemische Verteilungsgesetze der Elemente I–IX*, Norsk. Vid. Akad., Math.-Naturvid. Kl., Oslo **1923–1937**.
[6] G. T. Rado, H. Suhl in *Spin Arrangements and Crystal Structure, Domains, and Micromagnetics A Treatise on Modern Theory and Materials.* Academic Press, **2013**, p 5.
[7] a) G. Hodes, *Science* **2013**, *342*, 317–318; b) D. Dimos, C. H. Mueller, *Annu. Rev. Mater. Sci.* **1998**, *28*, 397–419; c) S. Park, T. R. Shrout, *IEEE T. Ultrason. Ferr.* **1997**, *44*, 1140–1147; d) F. S. Galasso in *Perovskites and High Tc Superconductors*, Gordon and Breach Science Publishers, New York, **1990**; e) L. G. Tejuca, J. L. G. Fierro (Eds.), *in Properties and applications of perovskite-type oxides*, Marcel Dekker Inc, New York, **1992**; f) K. D. Kreuer, *Ann. Rev. Mater. Res.* **2003**, *33*, 333–359; g) T. Ishihara (Ed.), in *Perovskite oxide for solid oxide fuel cells*, Springer, Dordrecht, **2009**; h) T. Qi, I. Grinberg, J. W. Bennett, Y.-H. Shin, A. M. Rappe, K.-L. Yeh, K. A. Nelson, *Inst. Electr. Electron Eng.* **2010**, 249–258.
[8] R. D. Rosenstein, R. Schoor, *J. Chem. Phys.* **1963**, *38*, 1789–1790.
[9] E. O. Kim, W. S. Kim, N. H. Hur, D. Jung, *Solid State Commun.* **2002**, *121*, 309–312.
[10] D. Stoiber, R. Niewa, *Z. Anorg. Allg. Chem.* **2019**, *645*, 329–334.
[11] M. Y. Chern, D. A. Vennos, F. J. DiSalvo, *J. Solid State Chem.* **1992**, *96*, 415–425.
[12] F. Gäbler, M. Kirchner, W. Schnelle, U. Schwarz, M. Schmitt, H. Rosner, R. Niewa, *Z. Anorg. Allg. Chem.* **2004**, *630*, 2292–2298.
[13] a) I. R. Shein, A. L. Ivanovskii, *Russ. J. Inorg. Chem.* **2003**, *48*, 711–719; b) I. R. Shein, A. L. Ivanovskii, *J. Solid State Chem.* **2004**, *177*, 61–64.
[14] M. T. Rahman, E. Haque, M. A. Hossain, *J. Alloys Compd.* **2019**, *783*, 593–600; E. Haque, M. A. Hossain, *J. Mater. Res.* in press.
[15] a) K. Kuhar, M. Pandey, K. S. Thygesen, K. W. Jacobsen, *ACS Energy Lett.* **2018**, *3*, 436–446; b) M. Rasukkannu, D. Velauthapillai, F. Bianchini, P. Vajeeston, *Materials* **2018**, *11*, 2006.
[16] a) W. F. Goh, W. E. Pickett, *Phys. Rev. B* **2018**, *97*, 035202; b) W. F. Goh, W. E. Pickett, *Phys. Rev. B* **2018**, *98*, 125147; c) C. K. Barman, C. Mondal, V. Singh, B. Pathak, A. Alam, *Phys. Rev. B* **2018**, *98*, 245149; d) Y. Sun, X.-Q. Chen, S. Yunoki, D. Li, Y. Li, *Phys. Rev. Lett.* **2010**, *105*, 216406; T. H. Hsieh, J. Liu, L. Fu, *Phys. Rev. B* **2014**, *90*, 081112(R).
[17] a) F. Gäbler, M. Kirchner, W. Schnelle, M. Schmitt, H. Rosner, R. Niewa, *Z. Anorg. Allg. Chem.* **2005**, *631*, 397–402; b) M. Pathak, D. Stoiber, M. Bobnar, A. Ormeci, Y. Prots, R. Niewa, P. Höhn, *Z. Anorg. Allg. Chem.* **2018**, *644*, 161–167.
[18] M. Y. Chern, F. J. DiSalvo, J. B. Parise, J. A. Goldstone, *J. Solid State Chem.* **1992**, *96*, 426–435.
[19] D. Stoiber, R. Niewa, *Z. Kristallogr.* **2019**, *234*, 201–209.
[20] a) A. Widera, H. Schäfer, *Mater. Res. Bull.* **1980**, *15*, 1805–1809; b) A. Widera, H. Schäfer, *J. Less-Common Met.* **1981**, *77*, 29–36.
[21] C. Röhr, *Z. Kristallogr.* **1995**, *210*, 781.
[22] R. Türck, Doctoral Thesis, Universität Stuttgart, Germany, **1996**.
[23] B. Huang, J. D. Corbett, *Z. Anorg. Allg. Chem.* **1998**, *624*, 1787–1790.
[24] A. Velden, M. Jansen, *Z. Anorg. Allg. Chem.* **2004**, *630*, 234–238.
[25] J. Nuss, C. Mühle, K. Hayama, V. Abdolazimi, H. Takagi, *Acta Crystallogr., Sect. B* **2015**, *71*, 300–312.
[26] R. Niewa, *Z. Anorg. Allg. Chem.* **2013**, *639*, 1699–1715.
[27] a) P. E. Rauch, A. Simon, *Angew. Chem. Int. Ed. Engl.* **1992**, *31*, 1519–1521; *Angew. Chem.* **1992**, *104*, 1505; b) V. Smetana, V. Babizhetskyy, G. V. Vajenine, A. Simon, *J. Solid State Chem.* **2007**, *180*, 1889–1893.
[28] F. Gäbler, R. Niewa, *Inorg. Chem.* **2007**, *46*, 859–865.
[29] F. Gäbler, Y. Prots, R. Niewa, *Z. Anorg. Allg. Chem.* **2007**, *633*, 93–97.
[30] F. Gäbler, D. Bräunling, A. Senyshyn, W. Schnelle, R. Niewa, *Z. Anorg. Allg. Chem.* **2010**, *636*, 1222–1228.

[31] D. A. Papaconstantopoulos, W. E. Picket, *Phys. Rev. B* **1992**, *45*, 4008–4012.
[32] F. Gäbler, D. Bräunling, W. Schnelle, I. Schellenberg, R. Pöttgen, R. Niewa, *Z. Anorg. Allg. Chem.* **2011**, *637*, 977–982.
[33] R. Niewa, W. Schnelle, F. R. Wagner, *Z. Anorg. Allg. Chem.* **2001**, *627*, 365–370.
[34] a) M. Kirchner, Diploma Thesis, Friedrich-Schiller-Universität Jena, Germany, **2001**; b) id., Doctoral Dissertation, Technische Universität Dresden, Germany, **2006**.
[35] K. Haddadi, A. Bouhemadou, L. Louail, *Solid State Commun.* **2010**, *150*, 932–937.
[36] J. Jäger, D. Stahl, P. C. Schmidt, R. Kniep, *Angew. Chem. Int. Ed. Engl.* **1993**, *32*, 709–710; *Angew. Chem.* **1993**, *105*, 738.
[37] R. Boča, R. Kniep, *Solid State Commun.* **1993**, *88*, 391–394.
[38] G.-Y. Adachi, N. Imanaka, Z. Fuzhong in *Handbook on the Physics and Chemistry of Rare Earths*, *Vol. 15* (Eds.: K. A. Gschneidner Jr., L. Eyring), Elsevier, Amsterdam **1991**.
[39] H. Haschke, H. Nowotny, F. Benesovsky, *Monatsh. Chem.* **1967**, *98*, 2157–2163.
[40] M. Kirchner, W. Schnelle, F. R. Wagner, R. Niewa, *Solid State Sci.* **2003**, *5*, 1247–1257.
[41] J.-T. Zhao, Z.-C. Dong, J. T. Vaughey, J. E. Ostenson, J. D. Corbett, *J. Alloys Compd.* **1995**, *230*, 1–12.
[42] F. Gäbler, W. Schnelle, A. Senyshyn, R. Niewa, *Solid State Sci.* **2008**, *10*, 1910–1915.
[43] A. S. Mikhaylushkin, C. Höglund, J. Birch, Z. Czigány, L. Hultman, S. I. Simak, B. Alling, F. Tasnádi, I. A. Abrikosov, *Phys. Rev. B* **2009**, *79*, 134107.
[44] V. Kanchana, S. Ram, *Intermetallics* **2012**, *23*, 39–48.
[45] M. A. Hossain, M. S. Ali, F. Parvin, A. K. M. A. Islam, *Comput. Mater. Sci.* **2013**, *73*, 1–8.
[46] V. Kanchana, S. Ram, *Solid State Commun.* **2014**, *181*, 54–59.
[47] N. Bettahar, D. Nasri, S. Benalia, M. Merabet, B. Abidri, N. Benkhettou, R. Khenata, D. Rached, M. Rabah, *Int. J. Thermophys.* **2013**, *34*, 434–449.
[48] S. Kacimin, D. Mekam, M. Djermouni, M. Azzouz, A. Hallouche, A. Zaoui, *Mater. Sci. Semicond. Process.* **2013**, *16*, 1971–1976.
[49] S. P. Yatsenko, A. A. Semyannikov, H. O. Shakarov, E. G. Fedorova, *J. Less-Common Met.* **1983**, *90*, 95–108.
[50] S. Delfino, A. Saccone, R. Ferro, *J. Less-Common Met.* **1984**, *102*, 289–310.
[51] N. Kurtzemann, H. Kohlmann, *Z. Anorg. Allg. Chem.* **2010**, *636*, 1032–1037.
[52] R. Niewa, D. A. Zherebtsov, M. Kirchner, M. Schmidt, W. Schnelle, *Chem. Mater.* **2004**, *16*, 5445–5451.
[53] R. D. Shannon, *Acta Crystallogr., Sect. A* **1976**, *32*, 751–767.
[54] M. Kirchner, W. Schnelle, R. Niewa, *Z. Anorg. Allg. Chem.* **2006**, *632*, 559–564.
[55] R. Niewa, Habilitation Thesis, Technische Universität Dresden, Germany, **2005**.
[56] P. Ravindran, R. Asokamani, *J. Phys. Condens. Matter* **1995**, *7*, 5567–5577.
[57] T. Dagerhamn, *Arkiv Kemi* **1967**, *27*, 363–379.
[58] A. Saccone, A. M. Cardinale, S. Delfino, R. Ferro, *Z. Metallkd.* **1996**, *87*, 82–87.
[59] J. H. N. van Vucht, *Z. Metallkd.* **1957**, *48*, 253–258.
[60] K. H. J. Buschow, J. H. N. van Vucht, *Z. Metallkd.* **1966**, *57*, 162–166.
[61] K. H. J. Buschow, *J. Less-Common Met.* **1965**, *9*, 452–456.
[62] K. H. J. Buschow, J. H. N. van Vucht, *Philips Res. Rep.* **1967**, *22*, 233–245.
[63] J. Sakurai, Y. Murashita, Y. Aoki, T. Fujita, T. Takabatake, H. Fujii, *J. Phys. Soc. Jpn.* **1989**, *58*, 4078–4085.
[64] K. H. Mader, W. E. Wallace, *J. Less-Common Met.* **1968**, *16*, 85–90.
[65] J. C. Schuster, *J. Less-Common Met.* **1985**, *105*, 327–332.
[66] C. Höglund, J. Birch, M. Beckers, B. Alling, Z. Czigán, A. Mücklich, L. Hultman, *Eur. J. Inorg. Chem.* **2008**, 1193–1195.
[67] J. C. Schuster, J. Bauer, H. Nowotny, *Rev. Chim. Minér.* **1985**, *22*, 546–554.
[68] M. Kirchner, F. Gäbler, W. Schnelle, F. R. Wagner, R. Niewa, *Z. Kristallogr.* **2006**, *221*, 543–553.
[69] a) W. Jeitschko, H. Nowotny, F. Benesovsky, *Monatsh. Chem.* **1964**, *95*, 1040–1043; b) H. Haschke, H. Nowotny, F. Benesovsky, *Monatsh. Chem.* **1966**, *97*, 1045.
[70] C. S. Garde, J. Ray, G. Chandra, *J. Alloys Compd.* **1993**, *198*, 165–172.
[71] M. Kirchner, W. Schnelle, R. Niewa, *Z. Naturforsch. B* **2006**, *61*, 813–819.
[72] M. Rahm, R. Hoffmann, N. W. Ashcroft, *Chem. Eur. J.* **2016**, *22*, 14625–14632.
[73] V. F. Buchwald, H. P. Nielsen, *Lunar Planet. Sci.* **1981**, *12*, 112–114.
[74] a) A. Fry, *Stahl Eisen* **1923**, *43*, 1271–1279; b) B. Prenosil, J. Holub, M. Koutnik, *Haerterei-Tech. Mitt.* **1973**, *28*, 157–164.
[75] G. Shirane, W. J. Takei, S. L. Ruby, *Phys. Rev.* **1962**, *126*, 49–52.
[76] T. K. Kim, M. Takahash, *Appl. Phys. Lett.* **1972**, *20*, 492–494.
[77] D. Andriamandroso, L. Fefilatiev, G. Demazeau, L. Fournes, M. Pouchard, *Mater. Res. Bull.* **1984**, *19*, 1187–1194.
[78] H. A. Wriedt, N. A. Gokcen, R. H. Nafziger, *Bull. Alloy Phase Diagrams* **1987**, *8*, 355–377.
[79] a) R. Niewa, D. Rau, A. Wosylus, K. Meier, M. Wessel, M. Hanfland, R. Dronskowski, U. Schwarz, *J. Alloys Compd.* **2009**, *480*, 76–80; b) K. Guo, D. Rau, J. von Appen, Y. Prots, W. Schnelle, R. Dronskowski, R. Niewa, U. Schwarz, *High Pressure Res.* **2013**, *33*, 684–696.
[80] a) R. Juza, H. Puff, F. Wagenknecht, *Z. Elektrochem.* **1957**, *61*, 804–809; b) R. Juza, *Adv. Inorg. Chem. Radiochem.* **1966**, *9*, 81–131; c) W. J. Takei, G. Shirane, R. R. Heikes, *Phys. Rev.* **1962**, *125*, 1893–1897; d) C. Guillaud, T. Wyart, *Rev. Metall.* **1948**, *45*, 271–276; e) R. Juza, H. Puff, *Z. Elektrochem.* **1957**, *61*, 810–819; f) W. J. Takei, G. Shirane, B. C. Frazer, *Phys. Rev.* **1960**, *119*, 122–126; g) S. K. Iyer, H. J. Grabke, *Arch. Eisenhüttenwes.* **1973**, *44*, 720.
[81] a) N. A. Gokcen, *Bull. Alloys Phase Diagrams* **1990**, *11*, 33–42; b) M. Widenmeyer, T. C. Hansen, A. Leineweber, A. Weidenkaff, R. Niewa, *Z. Anorg. Allg. Chem.* **2017**, *643*, 1929–1938.
[82] G. W. Wiener, J. A. Berger, *Trans. Am. Inst. Min. Metall. Pet. Eng.* **1955**, *203*, 360–368.
[83] a) M. Lourenco, M. Carvalho, P. Fonseca, T. Gasche, G. Evans, M. Godinho, M. Cruz, *J. Alloys Compd.* **2014**, *612*, 176–182; b) M. Widenmeyer, L. Shlyk, N. Becker, R. Dronskowski, E. Meissner, R. Niewa, *Eur. J. Inorg. Chem.* **2016**, 4792–4801; c) N. Pandey, M. Gupta, P. Rajput, J. Stahn, *J. Magn. Magn. Mater.* **2018**, *448*, 274–277; K. Oda, T. Yoshio, K. Oda, *J. Mater. Sci.* **1987**, *22*, 2729–2733.
[84] a) I. K. Milad, K. J. Smith, P. C. Wong, K. A. R. Mitchell, *Catal. Lett.* **1998**, *52*, 113–119; b) H. Cheng, Y. Huang, A. Wang, X. Wang, T. Zhang, *Top. Catal.* **2009**, *52*, 1535–1540; c) Z. Yao, A. Zhang, Y. Li, Y. Zhang, X. Cheng, C. Shi, *J. Alloys Compd.* **2008**, *464*, 488–496; d) Z. Yao, A. Zhu, C. T. Au, C. Shi, *Catal. Lett.* **2009**, *130*, 63–71; e) Z. Yao, X. Zhang, F. Peng, H. Yu, H. Wang, J. Yang, *Int. J. Hydrogen Energy* **2011**, *36*, 1955–1959; f) Y. Hu, H. Yang, J. Chen, T. Long, M. S. J. T. Balogun, Y. Tong, *ACS Appl. Mater. Interfaces* **2019**, *11*, 5152–5158.
[85] a) N. Terao, A. Bergghezan, *J. Phys. Soc. Jpn.* **1959**, *14*, 139–148; b) N. Terao, *Naturwissenschaften* **1959**, *6*, 20; c) N. Terao, A. Bergghezan, *J. Phys. Soc. Jpn.* **1960**, *15*, 227–230; d) S. Nagakura, N. Ōtsuka, Y. Hirotsu, *J. Phys. Soc. Jpn.* **1973**, *35*, 1492–1495.
[86] C. M. Fang, R. S. Koster, W. F. Li, M. A. van Huis, *RSC Adv.* **2014**, *4*, 7885–7899.
[87] A. Leineweber, S. B. Maisel, *Comput. Mater. Sci.* **2019**, *161*, 209–214.
[88] J. Blucher, K. Bang, B. C. Giessen, *Mater. Sci. Eng. A* **1989**, *117*, L1–L3.
[89] S. Matar, L. Fournes, S. Cherubinjeannette, G. Demazeau, *Eur. J. Solid State Inorg. Chem.* **1993**, *30*, 871–881.
[90] D. Xue, F. Li, J. Yang, Y. Kong, M. Gao, *J. Magn. Magn. Mater.* **1997**, *172*, 165–172.
[91] a) K. Ito, T. Sanai, Y. Yasutomi, T. Gushi, K. Toko, H. Yanagihara, M. Tsunoda, E. Kita, T. Suemasu, *J. Appl. Phys.* **2015**, *117*, 17B717; b) K. Ito, T. Sanai, Y. Yasutomi, S. Zhu, K. Toko, Y. Takeda, Y. Saitoh, A. Kimura, T. Suemasu, *J. Appl. Phys.* **2014**, *115*, 17C712.
[92] J. van Appen, R. Dronskowski, *Angew. Chem. Int. Ed.* **2005**, *44*, 1205–1210; *Angew. Chem.* **2005**, *117*, 1230.
[93] X. G. Ma, J. J. Jiang, P. Liang, J. Wang, Q. Ma, Q. K. Zhang, *J. Alloys Compd.* **2009**, *480*, 475–480.
[94] A. V. dos Santos, C. A. Kuhnen, *J. Alloys Compd.* **2001**, *321*, 60–66.
[95] Z. Wu, J. Meng, *Appl. Phys. Lett.* **2007**, *90*, 241901.
[96] Y. Takahashi, Y. Imai, T. Kumagai, *J. Magn. Magn. Mater.* **2011**, *323*, 2941–2944.
[97] X. G. Diao, F. S. Li, Z. J. Zhao, S. Q. Zhou, *J. Mater. Sci. Lett.* **1996**, *15*, 1590–1591.
[98] R. Loloee, *J. Appl. Phys.* **2012**, *112*, 023902.
[99] P. P. Mishra, M. M. Raja, R. N. Panda, *J. Supercond. Nov. Magn.* **2016**, *29*, 1347–1356.

[100] a) F. Takata, K. Ito, S. Higashikozono, T. Gushi, K. Toko, T. Suemasu, *J. Appl. Phys.* **2016**, *120*, 083907; b) X. G. Diao, A. Y. Takeuchi, F. Garcia, R. B. Scorzelli, H. R. Rechenberg, *J. Appl. Phys.* **1999**, *85*, 4485–4487.
[101] a) F. S. Li, Z. J. Zhao, X. D. Diao, D. S. Xue, *Phys. Status Solidi A* **1999**, *174*, 255–262; b) Y. Kong, F. Li, *Phys. Rev. B* **1998**, *57*, 970–977; c) Y. Q. Wu, M. F. Yan, *Phys. B* **2010**, *405*, 2700–2705; d) S. K. Chen, S. Jin, R. H. Tiefel, Y. F. Hsieh, E. M. Gyorgy, D. W. Johnson Jr., *J. Appl. Phys.* **1991**, *70*, 6247–6249.
[102] F. Takato, Y. Takeda, Y. Saitoh, K. Takanashi, A. Kimura, T. Suemasu, *Phys. Rev. Mater.* **2018**, *2*, 024407.
[103] P. Mohn, K. Schwarz, S. Matar, G. Demazeau, *Phys. Rev. B* **1992**, *45*, 4000–4007.
[104] F. Takata, K. Ito, T. Suemasu, *Jpn. J. Appl. Phys.* **2018**, *57*, 058004.
[105] B. Siberchicot, S. F. Matar, L. Fournes, G. Demazeau, P. Hagenmuller, *J. Solid State Chem.* **1990**, *84*, 10–15; J. Martínez, L. Lopardo, J. Desimoni, *J. Alloys Compd.* **2013**, *557*, 218–222.
[106] a) A. Anzai, T. Gushi, T. Komori, S. Honda, S. Isogami, T. Suemasu, *J. Appl. Phys.* **2018**, *124*, 123905; b) S. Isogami, A. Anzai, T. Gushi, T. Komori, T. Suemasu, *Jpn. J. Appl. Phys.* **2018**, *57*, 120305.
[107] a) L. Chen, *J. Appl. Phys.* **2006**, *100*, 113717; b) A. V. Gil Rebaza, A. M. Mudarra Navarro, J. Martinez, E. L. Peltzer y Blancá, *J. Alloys Compd.* **2016**, *683*, 32–37.
[108] C. A. Kuhnen, A. V. dos Santos, *J. Magn. Magn. Mater.* **1994**, *130*, 353–362.
[109] S. El Khiraoui, M. Sajieddine, M. Vergnat, P. Bauer, M. Mabrouki, *Phys. B* **2007**, *388*, 180–182.
[110] R. S. de Figueiredo, J. Foct, A. V. dos Santos, C. A. Kuhnen, *J. Alloys Compd.* **2001**, *315*, 42–50.
[111] R. S. de Figueiredo, C. A. Kuhnen, A. V. dos Santos, *J. Magn. Magn. Mater.* **1997**, *173*, 141–154.
[112] W. Wang, X. Kan, X. Liu, S. Feng, C. Liu, K. M. U. Rehman, M. Shezad, Q. Wu, Y. Wang, *J. Mater. Sci.* **2019**, *30*, 10383–10390.
[113] C. A. Kuhnen, R. S. de Figueiredo, A. V. dos Santos, *J. Magn. Magn. Mater.* **2000**, *219*, 58–68.
[114] a) Y. Fu, S. Lin, B. Wang, *J. Magn. Magn. Mater.* **2015**, *378*, 54–58; b) T. Scholz, A. Leineweber, R. Dronskowski, *J. Magn. Magn. Mater.* **2016**, *416*, 475–476.
[115] D. Andriamandroso, S. Matar, G. Demazeau, L. Fournes, *IEEE Trans. Magnetics* **1993**, *29*, 2–6.
[116] a) C. Paduani, *J. Magn. Magn. Mater.* **2004**, *278*, 231–236; b) J. C. Krause, C. Paduani, *Phys. B* **2005**, *367*, 282–286; c) S. F. Matar, A. Houari, M. A. Belkhir, M. Zakhour, *Z. Naturforsch. B* **2007**, *62*, 881–890; d) E. Zhao, H. Xiang, J. Meng, Z. Wu, *Chem. Phys. Lett.* **2007**, *449*, 96–100; e) A. V. dos Santos, C. A. Kuhnen, *J. Solid State Chem.* **2009**, *182*, 3183–3187; f) K. Hocine, M. Rabah, D. Rached, S. Djili, H. Baltache, *Comput. Mater. Sci.* **2012**, *65*, 6–12.
[117] a) C. Paduani, *Phys. Status Solidi B* **2004**, *241*, 2923–2927; b) A. V. dos Santos, *Comput. Mater. Sci.* **2012**, *56*, 108–115; c) . V. dos Santos, *J. Mater. Res.* **2014**, *29*, 959–974.
[118] a) A. Houben, P. Müller, J. von Appen, H. Lueken, R. Niewa, R. Dronskowski, *Angew. Chem. Int. Ed.* **2005**, *44*, 7212–7215; *Angew. Chem.* **2005**, *117*, 7379; b) A. Houben, V. Šepelák, K.-D. Becker, R. Dronskowski, *Chem. Mater.* **2009**, *21*, 784–788.
[119] a) C. Cordier-Robert, J. Foct, *Eur. J. Solid State Inorg. Chem.* **1992**, *29*, 39–51; b) H. H. Stadelmaier, A. C. Fraker, *Trans. Am. Inst. Min. Metall. Pet. Eng.* **1960**, *218*, 571–572; c) T. Takahashi, D. Music, J. M. Schneider, *J. Vac. Sci. Technol. A* **2012**, *30*, 030602; d) S. Matar, P. Mohn, J. Kübler, *J. Magn. Magn. Mater.* **1992**, *104–107*, 1927–1928; e) C. A. Kuhnen, A. V. dos Santos, *J. Alloys Compd.* **2000**, *297*, 68–72; f) D. Music, J. Burghaus, T. Takahashi, R. Dronskowski, J. M. Schneider, *Eur. Phys. J. B* **2010**, *77*, 401–406; g) A. V. dos Santos, G. Padilha, M. Monçalves, *Solid State Sci.* **2012**, *14*, 269–275.
[120] a) Z. Zhao, D. Xue, Z. Chen, F. Li, *Phys. Status Solidi A* **1999**, *174*, 249–253; b) Z. J. Zhao, D. S. Xue, F. S. Li, *J. Magn. Magn. Mater.* **2001**, *232*, 155–160.
[121] T. Scholz, R. Dronskowski, *Inorg. Chem.* **2015**, *54*, 8800–8807.
[122] a) T. Scholz, R. Dronskowski, *AIP Adv.* **2016**, *6*, 55107; b) S. Khmelevskyi, P. Mohn, *Phys. Rev. B* **2019**, *99*, 54405.
[123] H. Boller, *Monatsh. Chem.* **1968**, *99*, 2444–2449.
[124] H. H. Stadelmaier, A. C. Fraker, *Z. Metallkd.* **1962**, *53*, 48–51.
[125] a) T. Scholz, R. Dronskowski, *J. Mater. Chem. C* **2017**, *5*, 166–175; b) X. C. Kan, B. S. Wang, L. Zhang, L. Zu, S. Lin, J. C. Lin, P. Tong, W. H. Song, Y. P. Sun, *Phys. Chem. Chem. Phys.* **2017**, *19*, 13703–13709.
[126] Y. Yu, J. M. Elbicki, W. E. Wallace, S. Simizu, S. G. Sankar, *IEEE Trans. Magn.* **1992**, *28*, 2569–2571.
[127] T. Scholz, R. Dronskowski, *J. Mater. Chem. C* **2019**, *7*, 3822–3828.
[128] a) J. Burghaus, M. Wessel, A. Houben, R. Dronskowski, *Inorg. Chem.* **2010**, *49*, 10148–10155; b) A. V. Gil Rebaza, J. Desimoni, S. Kurian, S. Bhattacharyya, N. S. Gajbhiye, E. L. Peltzer y Blancá, *J. Phys. Chem. C* **2011**, *115*, 23081–23089; c) J. Burghaus, M. T. Sougrati, A. Möchel, A. Houben, R. P. Hermann, R. Dronskowski, *J. Solid State Chem.* **2011**, *184*, 2315–2321; d) M. Junaid, D. Music, M. Hans, J. M. Schneider, T. Scholz, R. Dronskowski, D. Primetzhofer, *J. Vac. Sci. Technol. A* **2016**, *34*, 40601.
[129] a) A. Houben, J. Burghaus, R. Dronskowski, *Chem. Mater.* **2009**, *21*, 4332–4338; b) A. Houben, J. Burghaus, R. Dronskowski, *Chem. Mater.* **2011**, *23*, 3580–3581.
[130] J. Burghaus, J. Kleemann, R. Dronskowski, *Z. Anorg. Allg. Chem.* **2011**, *637*, 935–939.
[131] H. H. Stadelmaier, T. S. Yun, *Z. Metallkd.* **1961**, *52*, 477–480.
[132] K. Takenaka, *Sci. Technol. Adv. Mater.* **2012**, *13*, 013001.
[133] R. Juza, K. Deneke, H. Puff, *Z. Elektrochem.* **1959**, *63*, 551–557.
[134] K. Takenaka, M. Ichigo, T. Hamada, A. Ozawa, T. Shibayama, T. Inagaki, K. Asano, *Sci. Technol. Adv. Mater.* **2014**, *15*, 15009.
[135] a) D. Fruchart, E. F. Bertaut, R. Matar, G. Lorthioir, R. Fruchart, *Solid State Commun.* **1971**, *9*, 1793–1797; b) D. Boldrin, E. Mendive-Tapia, J. Zemen, J. B. Staunton, T. Hansen, A. Aznar, J.-L. Tamarit, M. Barrio, P. Lloveras, J. Kim, X. Moya, L. F. Cohen, *Phys. Rev. X* **2018**, *8*, 041035.
[136] a) M. Wu, C. Wang, Y. Sun, L. Chu, J. Yan, D. Chen, Q. Huang, J. W. Lynn, *J. Appl. Phys.* **2013**, *114*, 123902; b) S. H. Deng, Y. Sun, H. Wu, Q. Huang, J. Yan, K. Shi, M. I. Malik, H. Lu, L. Wang, R. Huang, L. Li, C. Wang, *Chem. Mater.* **2015**, *27*, 2495–2501.
[137] D. Boldrin, A. P. Mihai, B. Zou, J. Zemen, R. Thompson, E. Ware, B. V. Neamtu, L. Ghivelder, B. Esser, D. W. McComb, P. Petrov, L. F. Cohen, *ACS Appl. Mater. Interfaces* **2018**, *10*, 18863–18868.
[138] R. Madar, L. Gilles, A. Rouault, J.-P. Bouchard, E. Fruchart, G. Lorthioir, R. Fruchart, *C. R. Acad. Sci. Paris* **1967**, *264*, 308–311.
[139] a) E. Krén, É. Zsoldos, M. Barberon, R. Fruchart, *Solid State Commun.* **1971**, *9*, 27–31; b) E. Krén, G. Kadar, M. M. Barberon, R. Fruchart, *Int. J. Magn.* **1971**, *1*, 341–344; c) S. Goumri-Said, M. Kanoun, F. Calvayrac, *J. Magn. Magn. Mater.* **2009**, *321*, 1012–1014; d) R. H. Chou, Y. Sun, H. Lu, G.-H. Lu, *Int. J. Mod. Phys. B* **2018**, *32*, 1850314.
[140] J. García, J. Bartolomé, D. González, R. Navarro, D. Fruchart, *J. Chem. Thermodyn.* **1983**, *15*, 1041–1057.
[141] a) Y. Sun, C. Wang, Q. Huang, Y. Guo, L. Chu, M. Arai, K. Yamaura, *Inorg. Chem.* **2012**, *51*, 7232–7236; b) Y. S. Sun, Y. F. Guo, X. X. Wang, Y. Tsujimoto, Y. Matsushita, Y. G. Shi, C. Wang, A. A. Belik, K. Yamaura, *Appl. Phys. Lett.* **2012**, *100*, 161907; c) S. Deng, Y. Sun, L. Wang, Z. Shi, H. Wu, Q. Huang, J. Yan, K. Shi, P. Hu, A. Zaoui, C. Wang, *J. Phys. Chem. C* **2015**, *119*, 24983–24990.
[142] a) D. Fruchart, E. F. Bertaut, *Proc. Intern. Conf. Magn.* **1974**, *4*, 572; b) W. J. Feng, D. LI, Q. Zhang, Y. F. Deng, S. Ma, Z. D. Zhang, *Mater. Sci. Poland* **2009**, *27*, 33–42.
[143] a) K. Asano, K. Koyama, K. Takenaka, *Appl. Phys. Lett.* **2008**, *92*, 161909; b) C. Yang, P. Tong, J. Lin, S. Lin, D. Cui, B. Wang, W. Song, W. Lu, Y. Sun, *J. Appl. Phys.* **2014**, *116*, 033902; c) R. Madar, M. Barberon, G. Lorthioi, E. Fruchart, R. Fruchart, *C. R. Seances Acad. Sci., Ser. C* **1968**, *267*, 1404–1406; d) E. O. Chi, W. S. Kim, N. H. Hur, *Solid State Commun.* **2001**, *120*, 307–310.
[144] a) P. Ettmayer, *Monatsh. Chem.* **1967**, *98*, 1881–1883; b) P. Ettmayer, G. Jangg, *Monatsh. Chem.* **1973**, *104*, 1120–1130.
[145] a) B. Song, J. Jian, H. Bao, M. Lei, H. Li, G. Wang, Y. Xu, X. Chen, *Appl. Phys. Lett.* **2008**, *92*, 192511; b) K. Takenaka, H. Takagi, *Appl. Phys. Lett.* **2005**, *87*, 261902; c) R. Navarro, J. A. Rojo, J. García, D. González, J. Bartolomé, P. l'Héritier, *J. Magn. Magn. Mater.* **1986**, *59*, 221–234; d) J. García, J. Bartolomé, D. González, R. Navarro, D. Fruchart, *J. Chem. Thermodyn.* **1983**, *15*, 1169–1180; e) J. García, R. Navarro, J. Bartolomé, R. Burriel, D. González, D. Fruchart, *J. Magn. Magn. Mater.* **1980**, *15–18*, 1155–1156; f) J. García, J. A. Rojo, R. Navarro, J. Bartolomé, D. González, *J. Magn. Magn. Mater.* **1983**, *31–34*, 1401–1403; g) J. García, D. González, J. Bartolomé, R. Navarro, J. A. Rojo, *J. Magn. Magn. Mater.* **1985**, *51*,

365–374; h) E. F. Bertaut, D. Fruchart, J. P. Bouchaud, R. Fruchart, *Solid State Commun.* **1968**, *6*, 251–256.
[146] M. Aoki, H. Yamane, M. Shimada, T. Kajiwara, *J. Alloys Compd.* **2004**, *364*, 280–282.
[147] D. Fruchart, P. L'Héritier, R. Fruchart, *Mater. Res. Bull.* **1980**, *15*, 415–420.
[148] J. C. Lin, B. S. Wang, P. Tong, W. J. Lu, L. Zhang, X. B. Zhu, Z. R. Yang, W. H. Song, J. M. Dai, Y. P. Sun, *Appl. Phys. Lett.* **2011**, *98*, 92507.
[149] Y. S. Sun, Y. F. Guo, X. X. Wang, W. Yi, J. J. Li, S. B. Zhang, C. I. Sathish, A. A. Belik, K. Yamaura, *J. Phys. Conf., Ser.* **2012**, *400*, 32094.
[150] M. Mekata, *J. Phys. Soc. Jpn.* **1962**, *17*, 796–803.
[151] M. Barberon, R. Madar, E. Fruchart, G. Lorthioir, R. Fruchart, *Mater. Res. Bull.* **1970**, *5*, 1–8.
[152] M. Nardin, C. Lorthioir, M. M. Barberon, R. Madar, E. Fruchart, R. Fruchart, *C. R. Acad. Sci. Paris* **1972**, *274*, 2168–2171.
[153] W. J. Feng, D. Li, W. J. Ren, Y. B. Li, W. F. Li, J. Li, Y. Q. Zhang, Z. D. Zhang, *J. Alloys Compd.* **2007**, *437*, 27–33.
[154] D. Fruchart, E. F. Bertaut, *J. Phys. Soc. Jpn.* **1978**, *44*, 781–791.
[155] M. Barberon, E. Fruchart, R. Fruchart, G. Lorthioir, R. Madar, M. Nardin, *Mater. Res. Bull.* **1972**, *7*, 109–118.
[156] a) T. Shimizu, T. Shibayama, K. Asano, K. Takenaka, *J. Appl. Phys.* **2012**, *111*, 7A903; b) Y. Sun, Y.-F. Guo, Y. Tsujimoto, X. Wang, J. Li, C. I. Sathish, C. Wang, K. Yamaura, *Adv. Condens. Matter Phys.* **2013**, 286325; c) Y. Sun, Y. Guo, Y. Tsujimoto, C. Wang, J. Li, X. Wang, H. L. Feng, C. I. Sathish, Y. Matsushita, K. Yamaura, *J. Appl. Phys.* **2014**, *115*, 43509.
[157] a) T. He, Q. Huang, A. P. Ramirez, Y. Wang, K. A. Regan, N. Rogado, M. A. Hayward, M. K. Haas, J. S. Slusky, K. Inumaru, H. W. Zandebergen, N. P. Ong, R. J. Cava, *Nature* **2001**, *411*, 54–46; b) B. He, C. Dong, L. Yang, X. Chen, L. Ge, L. Mu, Y. Shi, *Supercond. Sci. Technol.* **2013**, *26*, 125015; c) Z. Hui, X. Tang, D. Shao, H. Lei, J. Yang, W. Song, H. Luo, X. Zhu, Y. Sun, *Chem. Commun.* **2014**, *50*, 12734–12737; d) M. Uehara, A. Uehara, K. Kozawa, Y. Kimishima, *J. Phys. Soc. Jpn.* **2009**, *78*, 033702; e) P. Tong, Y. P. Sun, *Adv. Condens. Matter Phys.* **2012**, 903239.
[158] a) M. Uehara, A. Uehara, K. Kozawa, T. Yamazaki, Y. Kimishima, *Phys. C* **2010**, *470*, S688–S690; b) B. He, C. Dong, L. Yang, L. Ge, H. Chen, *J. Solid State Chem.* **2011**, *184*, 1939–1945.
[159] W. Cao, B. He, C. Liao, L. Yang, L. Zeng, C. Dong, *J. Solid State Chem.* **2009**, *182*, 3353–3357.
[160] T. S. Lehmann, B. Blaschkowski, R. Niewa, *Eur. J. Inorg. Chem.* **2019**, 1709–1713.
[161] D. Hirai, H. Tanaka, D. Nishio-Hamane, Z. Hiroi, *RSC Adv.* **2018**, *8*, 42025–42031.
[162] H. K. Singh, Z. Zhang, I. Opahle, D. Ohmer, Y. Yao, H. Zhang, *Chem. Mater.* **2018**, *30*, 6983–6991.
[163] L. Zu, S. Lin, J. Lin, B. Yuan, X. Kan, P. Tong, W. Song, Y. Sun, *Inorg. Chem.* **2016**, *55*, 9346–9351.
[164] H. Jacobs, U. Zachwieja, *J. Less-Common Met.* **1991**, *170*, 185–190.
[165] a) U. Hahn, W. Weber, *Phys. Rev. B* **1996**, *53*, 12684–12693; b) C. X. Quintela, N. Campbell, D. F. Shao, J. Irwin, D. T. Harris, L. Xie, T. J. Anderson, N. Reiser, X. Q. Pan, E. Y. Tsymbal, M. S. Rzchowski, C. B. Eom, *APL Mater.* **2017**, *5*, 096103.
[166] A. Ji, C. Li, Z. Cao, *Appl. Phys. Lett.* **2006**, *89*, 252120.
[167] a) N. Lu, A. Ji, Z. Cao, *Sci. Rep.* **2013**, *3*, 3090; b) L. Gao, A. Ji, W. Zhang, Z. Cao, *J. Cryst. Growth* **2011**, *321*, 157–161.
[168] a) G. Soto, I. Ponce, M. Moreno, F. Yubero, W. De la Cruz, *J. Alloys Compd.* **2014**, *594*, 48–51; b) I. Ponce-Cázaresa, G. Sotob, M. Guadalupe Moreno-Armenta, W. De la Cruz, *J. Alloys Compd.* **2015**, *641*, 216–222.
[169] F. Gulo, A. Simon, J. Köhler, R. K. Kremer, *Angew. Chem. Int. Ed.* **2004**, *43*, 2032–2034; *Angew. Chem.* **2004**, *116*, 2066.
[170] E. Lindahl, M. Ottosson, J.-O. Carlsson, *Thin Solid Films* **2018**, *647*, 1–8.
[171] a) M. P. Brady, D. T. Hoelzer, E. A. Payzant, P. F. Tortorelli, J. A. Horton, I. M. Anderson, L. R. Walker, S. K. Wrobel, *J. Mater. Res.* **2001**, *16*, 2784–2787; b) M. P. Brady, S. K. Wrobel, T. A. Lograsso, E. A. Payzant, D. T. Hoelzer, J. A. Horton, L. R. Walker, *Chem. Mater.* **2004**, *16*, 1984–1990.
[172] S. Lin, D. F. Shao, J. C. Lin, L. Zu, X. C. Kan, B. S. Wang, Y. N. Huang, W. H. Song, W. J. Lu, P. Tong, Y. P. Sun, *J. Mater. Chem. C* **2015**, *3*, 5683–5696.
[173] B. Wiendlocha, J. Tobola, S. Kaprzyk, D. Fruchart, *J. Alloys Compd.* **2007**, *442*, 289–291.
[174] a) H. M. Tütüncü, G. P. Srivastava, *J. Appl. Phys.* **2012**, *112*, 93914; b) K. M. Szczęśniak, R. Szczęśniak, D. Szczęśniak, K. A. Szewczyk, A. M. Duda, I. A. Domagalska, *Phys. C* **2017**, *541*, 10–15.
[175] C. Samson, J.-P. Bouchaud, R. Fruchard, *C. R. Acad. Sci. Paris* **1964**, *259*, 392–393.
[176] O. Beckmann, H. Boller, H. Nowotny, F. Benesovski, *Monatsh. Chem.* **1969**, *100*, 1465–1470.
[177] H. M. Tütüncü, G. P. Srivastava, *J. Appl. Phys.* **2013**, *114*, 53905.
[178] H. Boller, *Monatsh. Chem.* **1969**, *100*, 1471–1476.
[179] B. Wang, K. Ohgushi, *Sci. Rep.* **2016**, *6*, 37896.
[180] a) K. Takao, Z. Liu, K. Uji, T. Waki, Y. Tabata, I. Watanabe, H. Nakamura, *J. Phys. Conf., Ser.* **2017**, *868*, 12021; b) L. Zu, S. Lin, Y. Liu, J. C. Lin, B. Yuan, X. C. Kan, P. Tong, W. H. Song, Y. P. Sun, *Appl. Phys. Lett.* **2016**, *108*, 31906.
[181] a) T. Waki, K. Takao, Y. Tabata, H. Ohta, T. Yajima, Z. Hiroi, H. Nakamura, *J. Phys. Soc. Jpn.* **2017**, *86*, 104706; b) S. Lin, H. Lv, J. Lin, Y. Huang, L. Zhang, W. Song, P. Tong, W. Lu, Y. Sun, *Phys. Rev. B* **2018**, *98*, 14412.
[182] a) J. C. Schuster, J. Bauer, *J. Solid State Chem.* **1984**, *53*, 260–265; b) D. Vogtenhuber-Pawelczak, P. Herzig, *J. Solid State Chem.* **1992**, *99*, 85–94; c) A. L. Ivanovskii, N. I. Medvedeva, D. L. Novikov, *Phys. Solid State* **1997**, *39*, 929–931; d) V. Kanchana, *Europhys. Lett.* **2009**, *87*, 26006; e) D. Cherrad, L. Selmani, D. Maouche, M. Maamache, *J. Alloys Compd.* **2011**, *509*, 4357–4362; f) J. Wang, Z. Chen, C. Li, F. Li, C. Nie, *J. Solid State Chem.* **2014**, *216*, 1–8.
[183] a) W. Jeitschko, H. Nowotny, F. Benesovsky, *Monatsh. Chem.* **1964**, *95*, 436–438; b) K. Chen, C. Li, M. Hu, X. Hou, C. Li, Z. Chen, *Materials* **2017**, *10*, 362.
[184] W. Rieger, H. Nowotny, F. Benesovs, *Monatsh. Chem.* **1965**, *96*, 232–241.
[185] G. Serghiou, C. L. Guillaume, A. Thomson, J. P. Morniroli, D. J. Frost, *J. Am. Chem. Soc.* **2009**, *131*, 15170–15175.
[186] T. Scholz, A. L. Görne, R. Dronskowski, *Prog. Solid State Chem.* **2018**, *51*, 1–18.
[187] E. Lehrer, *Z. Elektrochem.* **1930**, *36*, 383–392.
[188] X. Liu, N. Fechler, M. Antonietti, *Chem. Soc. Rev.* **2013**, *42*, 8237–8265.
[189] T. S. Lehmann, R. Niewa, *Eur. J. Inorg. Chem.* **2019**, 730–734.
[190] T. S. Lehmann, Doctoral Dissertation, Universität Stuttgart, Germany, **2019**.
[191] D. D. Vaughn, J. Araujo, P. Meduri, J. F. Callejas, M. A. Hickner, R. E. Schaak, *Chem. Mater.* **2014**, *26*, 6226–6232.

Received: July 10, 2019